Shultz, L.D., Lyons, B.L., Burzenski, L.M., Gott, B., Chen, X., Chaleff, S., Kotb, M., Gillies, S.D., King, M., Mangada, J., et al. (2005). Human lymphoid and myeloid cell development in NOD/LtSz-scid IL2R gamma null mice engrafted with mobilized human hemopoietic stem cells. J. Immunol. *174*, 6477–6489.

So, C.W., Karsunky, H., Passegué, E., Cozzio, A., Weissman, I.L., and Cleary, M.L. (2003). MLL-GAS7 transforms multipotent hematopoietic progenitors and induces mixed lineage leukemias in mice. Cancer Cell *3*, 161–171.

Stevenson, F.K., and Caligaris-Cappio, F. (2004). Chronic lymphocytic leukemia: revelations from the B-cell receptor. Blood *103*, 4389–4395.

Sthoeger, Z.M., Wakai, M., Tse, D.B., Vinciguerra, V.P., Allen, S.L., Budman, D.R., Lichtman, S.M., Schulman, P., Weiselberg, L.R., and Chiorazzi, N. (1989). Production of autoantibodies by CD5-expressing B lymphocytes from patients with chronic lymphocytic leukemia. J. Exp. Med. *169*, 255–268.

Suljagic, M., Longo, P.G., Bennardo, S., Perlas, E., Leone, G., Laurenti, L., and Efremov, D.G. (2010). The Syk inhibitor fostamatinib disodium (R788) inhibits tumor growth in the Eμ- TCL1 transgenic mouse model of CLL by blocking antigen-dependent B-cell receptor signaling. Blood *116*, 4894–4905.

Terstappen, L.W., Huang, S., Safford, M., Lansdorp, P.M., and Loken, M.R. (1991). Sequential generations of hematopoietic colonies derived from single nonlineage-committed CD34+CD38- progenitor cells. Blood *77*, 1218–1227.

Tobin, G., Thunberg, U., Johnson, A., Eriksson, I., Söderberg, O., Karlsson, K., Merup, M., Juliusson, G., Vilpo, J., Enblad, G., et al. (2003). Chronic lymphocytic leukemias utilizing the VH3-21 gene display highly restricted Vlambda2-14 gene use and homologous CDR3s: implicating recognition of a common antigen epitope. Blood *101*, 4952–4957.

Tobin, G., Thunberg, U., Karlsson, K., Murray, F., Laurell, A., Willander, K., Enblad, G., Merup, M., Vilpo, J., Juliusson, G., et al. (2004). Subsets with restricted immunoglobulin gene rearrangement features indicate a role for antigen selection in the development of chronic lymphocytic leukemia. Blood *104*, 2879–2885.

van Dongen, J.J., Langerak, A.W., Brüggemann, M., Evans, P.A., Hummel, M., Lavender, F.L., Delabesse, E., Davi, F., Schuuring, E., García-Sanz, R., et al. (2003). Design and standardization of PCR primers and protocols for detection of clonal immunoglobulin and T-cell receptor gene recombinations in suspect lymphoproliferations: report of the BIOMED-2 Concerted Action BMH4-CT98-3936. Leukemia *17*, 2257–2317.

Widhopf, G.F., 2nd, Rassenti, L.Z., Toy, T.L., Gribben, J.G., Wierda, W.G., and Kipps, T.J. (2004). Chronic lymphocytic leukemia B cells of more than 1% of patients express virtually identical immunoglobulins. Blood *104*, 2499–2504.

Zenz, T., Mertens, D., Küppers, R., Döhner, H., and Stilgenbauer, S. (2010). From pathogenesis to treatment of chronic lymphocytic leukaemia. Nat. Rev. Cancer *10*, 37–50.

Published June 27, 2011

Phosphoinositide 3-kinase signaling pathway mediated by p110α regulates invadopodia formation

Hideki Yamaguchi,[1,2,3] Shuhei Yoshida,[2] Emi Muroi,[1,2] Nachi Yoshida,[1,2] Masahiro Kawamura,[2] Zen Kouchi,[2] Yoshikazu Nakamura,[2] Ryuichi Sakai,[1] and Kiyoko Fukami[2]

[1]Division of Metastasis and Invasion Signaling, National Cancer Center Research Institute, Chuo-ku, Tokyo 104-0045, Japan
[2]Laboratory of Genome and Biosignal, Tokyo University of Pharmacy and Life Sciences, Hachioji, Tokyo 192-0392, Japan
[3]Precursory Research for Embryonic Science and Technology, Japan Science and Technology Agency, Kawaguchi, Saitama 332-0012, Japan

Invadopodia are extracellular matrix–degrading protrusions formed by invasive cancer cells that are thought to function in cancer invasion. Although many invadopodia components have been identified, signaling pathways that link extracellular stimuli to invadopodia formation remain largely unknown. We investigate the role of phosphoinositide 3-kinase (PI3K) signaling during invadopodia formation. We find that in human breast cancer cells, both invadopodia formation and degradation of a gelatin matrix were blocked by treatment with PI3K inhibitors or sequestration of D-3 phosphoinositides. Functional analyses revealed that among the PI3K family proteins, the class I PI3K catalytic subunit p110α, a frequently mutated gene product in human cancers, was selectively involved in invadopodia formation. The expression of p110α with cancerous mutations promoted invadopodia-mediated invasive activity. Furthermore, knockdown or inhibition of PDK1 and Akt, downstream effectors of PI3K signaling, suppressed invadopodia formation induced by p110α mutants. These data suggest that PI3K signaling via p110α regulates invadopodia-mediated invasion of breast cancer cells.

Introduction

Degradation of ECM that is present in the basement membrane and tumor stroma is essential for local invasion and formation of metastatic sites by malignant cancer cells (Kessenbrock et al., 2010). Invadopodia, which were first described by Chen (1989), are ECM-degrading membrane protrusions formed on the ventral surface of invasive cancer cells and are thought to play a role in cancer cell invasion (Yamaguchi et al., 2005b; Weaver, 2006; Buccione et al., 2009; Madsen and Sahai, 2010). Invadopodia have been observed in a variety of invasive cancer cell lines, including mammary adenocarcinoma, colon carcinoma, melanoma, and glioma as well as in primary invasive tumor cells derived from glioblastoma and head and neck cancers (Clark et al., 2007; Stylli et al., 2008). In the case of breast cancer cell lines, the ability to form invadopodia is closely related to their invasive and metastatic properties in vivo (Coopman et al., 1998; Yamaguchi et al., 2005a, 2009). Additionally, invadopodia-like protrusions in breast cancer cells have been observed during intravasation by intravital imaging (Condeelis and Segall, 2003; Yamaguchi et al., 2005b). A recent study showed that invasive cancer cells use invadopodia to breach the basement membrane and penetrate into the stroma (Schoumacher et al., 2010). Moreover, Eckert et al. (2011) recently reported that Twist, an inducer of epithelial–mesenchymal transition, induces invadopodia formation to promote tumor metastasis and provided evidence of invadopodia formation in vivo in sections of invasive primary tumors.

Many components of invadopodia, such as various proteins involved in actin polymerization, cell signaling, membrane trafficking, cell–ECM adhesion, and ECM degradation, have been reported to date (Linder, 2007; Gimona et al., 2008; Caldieri and Buccione, 2010). We and other researchers previously reported that invadopodia formation is induced by stimulation with serum and growth factors (Tague et al., 2004;

Correspondence to Hideki Yamaguchi: hidyamag@ncc.go.jp

Abbreviations used in this paper: KD, kinase dead; Myr, myristoylated; PDK1, 3-phosphoinositide-dependent protein kinase-1; PH, pleckstrin homology; PI(3,4)P_2, phosphatidylinositol 3,4-bisphosphate; PI(3,4,5)P_3, phosphatidylinositol 3,4,5-trisphosphate; PI3K, phosphoinositide 3-kinase; shRNA, short hairpin RNA; WT, wild type.

© 2011 Yamaguchi et al. This article is distributed under the terms of an Attribution–Noncommercial–Share Alike–No Mirror Sites license for the first six months after the publication date (see http://www.rupress.org/terms). After six months it is available under a Creative Commons License (Attribution–Noncommercial–Share Alike 3.0 Unported license, as described at http://creativecommons.org/licenses/by-nc-sa/3.0/).

Supplemental Material can be found at:
http://jcb.rupress.org/content/suppl/2011/06/24/jcb.201009126.DC1.html

The Rockefeller University Press $30.00
J. Cell Biol. Vol. 193 No. 7 1275–1288
www.jcb.org/cgi/doi/10.1083/jcb.201009126

THE JOURNAL OF CELL BIOLOGY

Downloaded from jcb.rupress.org on May 17, 2012

Published June 27, 2011

Yamaguchi et al., 2005a; Mandal et al., 2008; Eckert et al., 2011). However, the signaling pathways that link these extracellular stimuli to invadopodia formation remain largely unknown.

The phosphoinositide 3-kinases (PI3Ks) are a family of lipid kinases that phosphorylate phosphoinositides at the D-3 position of the inositol headgroup and, thus, produce D-3 phosphoinositides (Cantley, 2002). PI3Ks mediate the signal transduction of extracellular stimuli and regulate diverse cellular events, such as mitogenesis, survival, membrane transport, and cell migration (Engelman et al., 2006; Cain and Ridley, 2009). PI3Ks are subdivided into three general classes (I–III) in mammals on the basis of their enzyme domain structures and substrate specificities (Fruman et al., 1998). Specifically, the class I subfamily consists of four catalytic subunits, including three class IA subunits (p110α, p110β, and p110δ) and a single class IB subunit (p110γ). However, the class II PI3K group consists of three isoforms, PI3K-C2α, PI3K-C2β, and PI3K-C2γ. Finally, mammals have a single class III isoform, namely, Vps34, which is a homologue of the sole PI3K present in yeast.

Uncontrolled activation of the PI3K signaling pathway leads to several pathological phenomena, including tumorigenesis and tumor malignancy (Cantley, 2002). This is indicated by the finding that the expression and activity of several members of the PI3K signaling pathway are frequently altered in a variety of human cancers (Yuan and Cantley, 2008). For instance, the *PIK3CA* gene, which encodes the class IA PI3K catalytic subunit p110α, is one of the most frequently amplified and mutated genes identified in human cancers (Yuan and Cantley, 2008; Zhao and Vogt, 2008). Clinical studies involving human breast cancer patients revealed that mutations leading to the activation of *PIK3CA* are associated with the development of invasive and metastatic phenotypes and poor patient prognosis (Saal et al., 2005; Li et al., 2006; Maruyama et al., 2007). Moreover, a previous study has shown that introduction of the mutant *PIK3CA* gene into a breast cancer cell line enhanced lung metastasis in mice (Pang et al., 2009). However, the detailed mechanisms by which the *PIK3CA* gene product p110α contributes to cancer invasion and metastasis are yet to be determined.

It is established that 3-phosphoinositide–dependent protein kinase-1 (PDK1) is a serine/threonine kinase that mediates PI3K signaling during various cellular responses (Toker and Newton, 2000). PDK1 is recruited to cell membranes upon PI3K activation, where it phosphorylates and activates Akt, the major mediator of the PI3K signaling pathway (Stephens et al., 1998). Both PDK1 and Akt are overexpressed in human breast cancers and are thought to be critical components of the oncogenic PI3K signaling pathway (Dillon et al., 2007; Maurer et al., 2009; Sheng et al., 2009). Furthermore, previous studies have demonstrated that PDK1 and Akt are involved in the invasive and metastatic phenotypes of human cancer cells (Xie et al., 2006; Dillon et al., 2007; Liu et al., 2009; Sheng et al., 2009). However, the roles of PDK1 and Akt in invadopodia formation remain unclear. In the present study, we investigate the role of PI3K signaling during invadopodia formation in invasive human breast cancer cells.

Results

PI3K activity is required for invadopodia formation in human breast cancer cells

The formation of invadopodia in human cancer cells and podosomes, which are structures functionally similar to invadopodia, in Src-transformed fibroblasts requires the activity of PI3K (Nakahara et al., 2003; Mandal et al., 2008; Oikawa et al., 2008). In the present study, the role of PI3K in invadopodia formation was investigated in detail in the highly invasive human breast cancer cell line MDA-MB-231 (Neve et al., 2006). MDA-MB-231 cells form invadopodia in vitro and have, therefore, been widely used in studies investigating various aspects of these invasive structures (Chen et al., 1994). MDA-MB-231 cells were seeded onto fluorescent gelatin-coated coverslips in the presence or absence of each of two PI3K inhibitors, LY294002 and wortmannin, and stained for two invadopodia markers, cortactin and F-actin. Invadopodia were observed as dotlike clusters of cortactin and F-actin on the ventral membrane of cells, which corresponded with the degradation sites on the gelatin matrix (Fig. S1 A). To quantify the invadopodia-mediated degradation of the gelatin matrix for each treatment, we calculated the area of the degradation sites. Both LY294002 and wortmannin significantly inhibited the formation of invadopodia and gelatin degradation in a dose-dependent manner, with half-maximal inhibitory concentration (IC_{50}) values of 3.3 μM and 3.6 nM for LY294002 and wortmannin, respectively (Fig. S1, B–D). Furthermore, the percentage of cells with invadopodia and the number of invadopodia per cell were also reduced in cells treated with either PI3K inhibitor (Fig. S1, E and F).

We also examined the effect of PI3K inhibition on the stability of preformed invadopodia. MDA-MB-231 cells expressing GFP-actin were seeded onto plates coated with a gelatin matrix, and cells were observed using time-lapse microscopy upon treatment with LY294002. LY294002 treatment of cells exhibiting GFP-actin–positive invadopodia resulted in the degradation of invadopodia within 1 min of treatment (Fig. S1 G and Video 1). A similar result was obtained when cells expressing Venus-cortactin were analyzed in the same manner (Video 2). Quantification of the intensity of GFP-actin signals at the invadopodia revealed that the actin core structures of invadopodia disassembled immediately after the addition of LY294002, whereas the invadopodia of cells treated with DMSO did not disassemble (Fig. S1 H). Collectively, these results indicate that PI3K activation is required for both the formation and stability of invadopodia in human breast cancer cells.

D-3 phosphoinositides are required for invadopodia formation

We next investigated the role of D-3 phosphoinositides synthesized by PI3Ks in invadopodia formation. The pleckstrin homology (PH) domain of Akt interacts with phosphatidylinositol 3,4,5-trisphosphate ($PI(3,4,5)P_3$) and phosphatidylinositol 3,4-bisphosphate ($PI(3,4)P_2$), which are two major products of PI3K, and its overexpression results in the sequestration and inhibition of the function of these phosphoinositides (Várnai et al., 2005). In the present study, the PH domain of Akt was

Downloaded from jcb.rupress.org on May 17, 2012

Published June 27, 2011

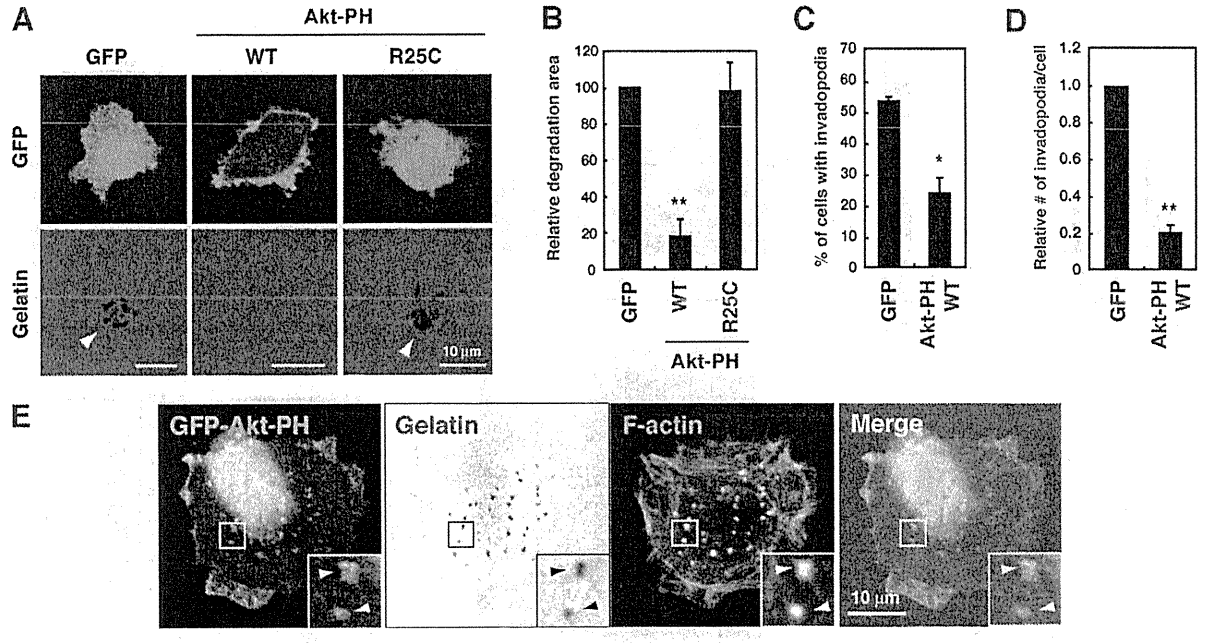

Figure 1. **D-3 phosphoinositides are necessary for invadopodia formation.** (A) MDA-MB-231 cells transfected with the GFP, GFP-Akt-PH wild-type (WT), or GFP-Akt-PH R25C mutant construct were cultured on fluorescent gelatin-coated coverslips for 7 h and imaged by confocal microscopy. Arrowheads denote degradation sites on the gelatin matrix. (B–D) Degraded areas on the gelatin matrix (B), the percentage of cells with invadopodia (C), and the relative number of invadopodia per cell (D) were quantified for transfected cells as described in the Materials and methods. (E) MDA-MB-231 cells stably expressing GFP-Akt-PH WT were cultured on fluorescent gelatin-coated coverslips for 3 h, stained for F-actin, and observed by confocal microscopy. Insets are magnified images of the boxed regions. Arrowheads denote invadopodia where GFP-Akt-PH signals were accumulated. Data in B–D are represented as means + SEM of four independent determinations. *, $P < 0.01$; and **, $P < 0.005$ by Student's *t* test.

overexpressed in MDA-MB-231 cells as a GFP fusion protein (GFP-Akt-PH). This construct, which localized to the plasma membrane, inhibited the formation of invadopodia, as measured by both the percentage of cells with invadopodia and the number of invadopodia per cell, and gelatin degradation (Fig. 1, A–D). In contrast, a mutant form of the Akt PH domain (R25C), in which an essential amino acid for phosphoinositide binding is mutated (Várnai et al., 2005), did not localize to the plasma membrane or inhibit gelatin degradation (Fig. 1, A and B). Furthermore, to examine the localization of D-3 phosphoinositides at invadopodia sites, a cell line expressing the GFP-Akt-PH construct at an extremely low level, ~13 times less than transient expression (Fig. S2 A), was established, which allows the cells to retain invadopodia. In these cells, signals corresponding to GFP-Akt-PH were significantly concentrated at F-actin–rich invadopodia and at the gelatin degradation sites (Fig. 1 E). This accumulation of GFP signals at invadopodia was not observed when cells expressing GFP alone were examined in the same manner (Fig. S2 B). These results indicate that $PI(3,4,5)P_3$ and/or $PI(3,4)P_2$ produced as downstream effectors of PI3K have an essential role in invadopodia-mediated ECM degradation.

The class I PI3K catalytic subunit p110α is an essential regulator of invadopodia formation

Mammalian cells contain eight PI3K enzymes, which are further classified into classes I, II, and III (Fruman et al., 1998). In the present study, the expression levels of the PI3K family of proteins were examined in MDA-MB-231 cells by real-time quantitative PCR and standard semiquantitative PCR analyses performed using different sets of primers specific for the PI3K isoforms (Fig. 2 A and Fig. S3 A). The class I subunits p110α, p110β, and p110δ, the class II subunit C2α, and the class III subunit Vps34 were abundantly expressed in these cells. Furthermore, the expression of the class II subunit C2β was weak but detectable. However, these cells did not express the class I subunit p110γ or the class II subunit C2γ.

siRNA knockdown experiments were performed to determine the contribution of individual PI3K isoforms to invadopodia formation. MDA-MB-231 cells were transfected with siRNAs targeting each PI3K enzyme and subsequently examined for invadopodia formation and gelatin degradation. The efficiency and selectivity of the siRNAs in knocking down individual PI3K isoforms were confirmed by RT-PCR analysis (Fig. 2 B), and the knockdown of class I p110 enzymes was also confirmed by immunoblotting (Fig. 2 C). Cells with reduced p110α levels showed a significant decrease in invadopodia formation and gelatin degradation activity (Fig. 2, D–G). Similar results were obtained with three other siRNAs targeting different regions of the p110α gene (Fig. S4, A and B). However, cells transfected with siRNAs targeting other class I PI3K enzymes (i.e., p110β and p110δ) did not show decreased invadopodia formation or gelatin degradation activity (Fig. 2, D and E). Furthermore, knockdown of classes II and III PI3Ks, including C2α, C2β, and Vps34, did not affect gelatin degradation activity (Fig. 2 D). Examination of the localization of endogenous p110α by immunocytochemistry revealed the presence of strong signals corresponding to endogenous p110α at invadopodia that were

Downloaded from jcb.rupress.org on May 17, 2012

Published June 27, 2011

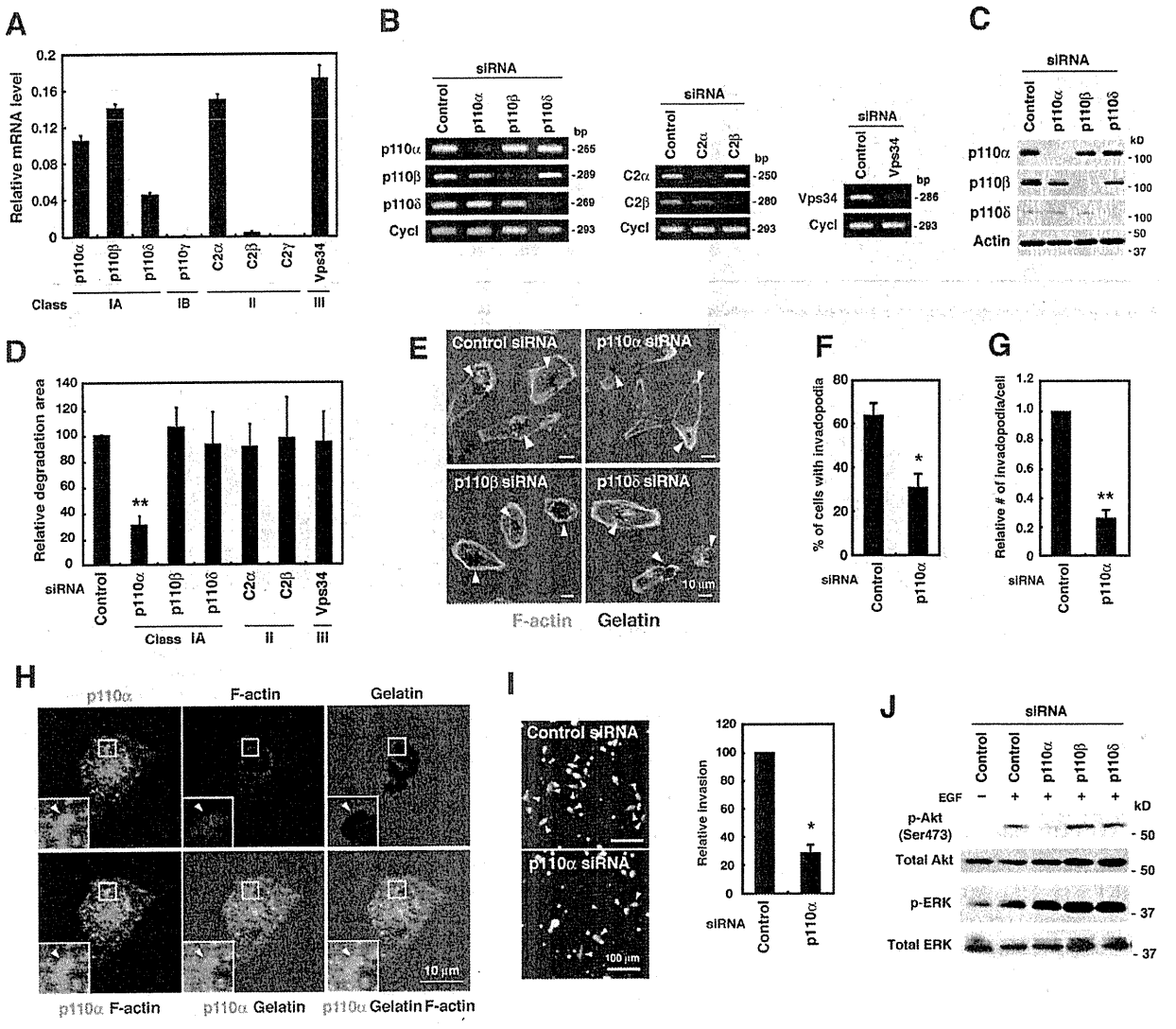

Figure 2. **Class I PI3K catalytic subunit p110α is an essential regulator of invadopodia formation.** (A) Real-time quantitative PCR analysis of the expression of PI3K isoforms in MDA-MB-231 cells. The relative mRNA levels of PI3K isoforms normalized with the mRNA levels of cyclophilin B are shown. (B and C) MDA-MB-231 cells were transfected with siRNAs targeting individual PI3K isoforms for 48 h, and the expression profiles of PI3K isoforms were determined by RT-PCR (B) and immunoblot analyses (C). Cyclophilin B (Cycl) and β-actin were used as internal controls. (D) MDA-MB-231 cells transfected with the indicated siRNAs were cultured on fluorescent gelatin-coated coverslips for 7 h, and the degraded areas on the gelatin matrix were quantified. (E) Representative images of cells transfected with siRNAs targeting p110 isoforms and stained for F-actin. Arrowheads denote the gelatin degradation sites. (F and G) The percentage of cells with invadopodia (F) and the relative number of invadopodia per cell (G) were determined in cells transfected with control or p110α siRNA. (H) MDA-MB-231 cells plated onto fluorescent gelatin-coated coverslips for 4 h were stained with anti-p110α antibody and phalloidin. Insets are magnified images of the boxed regions. Arrowheads denote accumulation of p110α signals at invadopodia. (I) MDA-MB-231 cells transfected with control or p110α siRNA were labeled with CellTracker green and analyzed for invasion through Matrigel-coated Transwell inserts for 24 h. Invaded cells were then imaged by fluorescent microscopy and counted. Arrowheads denote invaded cells. Smaller dots represent pores of the membrane of Transwell inserts. (J) MDA-MB-231 cells transfected with the indicated siRNAs were serum-starved overnight and stimulated with 8 nM EGF for 10 min. The cells were then analyzed by immunoblotting to determine the phosphorylation status of Akt (p-Akt) and ERK (p-ERK). Data are represented as means + SEM of three (A and I), eight (D), and five (F and G) independent determinations. *, $P < 0.01$; and **, $P < 0.0002$ by Student's *t* test.

enriched with F-actin and were associated with gelatin degradation sites (Fig. 2 H). To ascertain whether invadopodia formation mediated by p110α reflects the invasiveness of cancer cells, an in vitro Matrigel invasion assay was performed. MDA-MB-231 cells transfected with p110α siRNA showed markedly reduced invasion through Matrigel in comparison to cells transfected with control siRNA (Fig. 2 I). Collectively, these results indicate that among the PI3K family proteins, p110α is specifically involved in invadopodia-mediated invasion of human breast cancer cells.

The effect of p110α knockdown on invadopodia formation was assessed in other invasive breast cancer cell lines, namely BT-549 and Hs578T. BT-549 cells treated with two different p110α siRNAs showed a significant decrease in invadopodia-mediated gelatin degradation (Fig. S4, C and D). As Hs578T cells were sensitive to siRNA transfection under the present

Downloaded from jcb.rupress.org on May 17, 2012

Published June 27, 2011

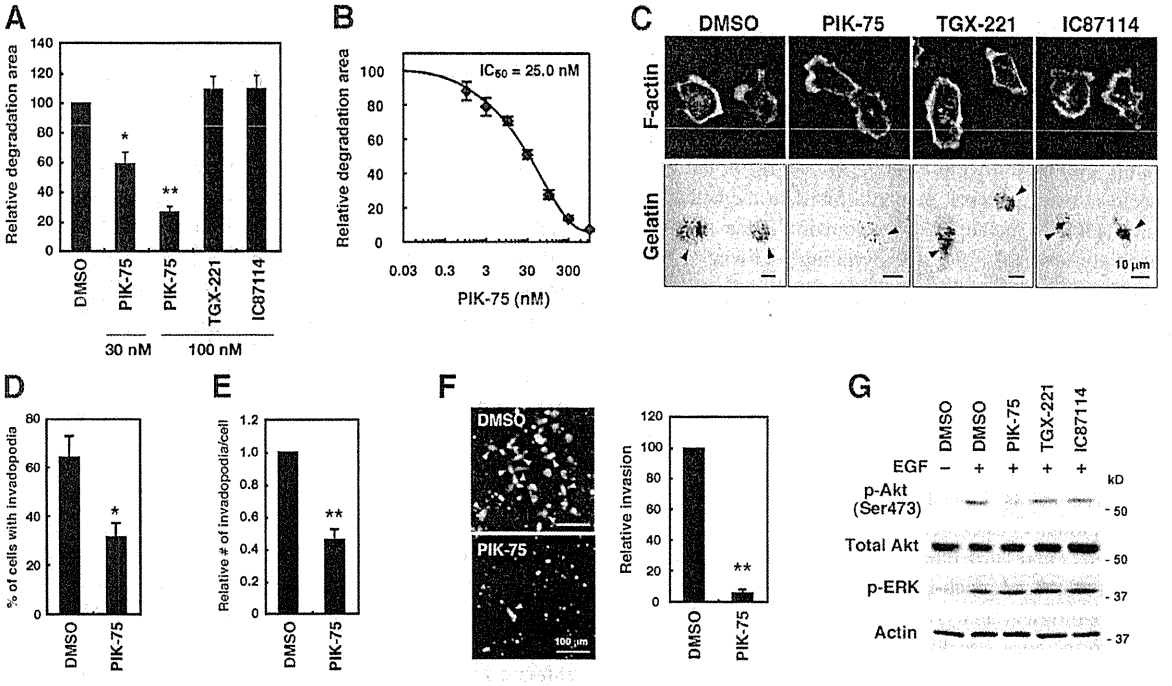

Figure 3. **Effects of pharmacological inhibition of class I PI3Ks on invadopodia formation.** (A) MDA-MB-231 cells were cultured on fluorescent gelatin-coated coverslips for 7 h in the presence or absence of various class I PI3K inhibitors, including PIK-75 for p110α, TGX-221 for p110β, and IC87114 for p110δ. The degraded areas on the gelatin matrix were quantified and are represented as the percentage of control DMSO-treated cells. (B) Dose–response curve of gelatin degradation obtained in the presence of increasing concentrations of PIK-75 is shown. (C) Representative images of MDA-MB-231 cells treated with various class I PI3K inhibitors are shown. Arrowheads denote the gelatin degradation sites. (D and E) The percentage of cells with invadopodia (D) and the relative number of invadopodia per cell (E) were determined in cells treated with control DMSO or 100 nM PIK-75. (F) MDA-MB-231 cells labeled with CellTracker green were analyzed for invasion through Matrigel-coated Transwell inserts in the presence or absence of 100 nM PIK-75 for 24 h. Invaded cells were then imaged by fluorescent microscopy and counted. Arrowheads denote invaded cells. (G) MDA-MB-231 cells were serum-starved overnight and treated with 300 nM of the indicated class I PI3K inhibitors for 1 h. The cells were subsequently stimulated with 8 nM EGF for 10 min and used for immunoblotting to determine the phosphorylation status of Akt (p-Akt) and ERK (p-ERK). Data are represented as means ± SEM of six (A, D, and E) and three (B and F) independent determinations. *, $P < 0.01$; and **, $P < 0.0005$ by Student's *t* tests.

experimental conditions, a short hairpin RNA (shRNA) targeting the p110α gene was introduced into Hs578T cells by lentiviral transduction. Transduction of Hs578T cells with p110α shRNA resulted in a marked reduction of the expression of p110α and a concomitant decrease in gelatin degradation activity as compared with cells with control shRNA (Fig. S4, E–G).

The PI3K signaling pathway activation status was determined by measuring the amount of phosphorylated Akt, a major downstream effector of the PI3K signaling pathway. Knockdown of p110α suppressed Akt phosphorylation upon EGF stimulation (Fig. 2 J), whereas knockdown of p110β or p110δ had almost no effect. Thus, p110α is likely the primary mediator of growth factor–stimulated PI3K signaling in this cell type. Importantly, EGF-induced phosphorylation of ERK was not affected by p110α knockdown (Fig. 2 J). This result suggests that p110α inhibition does not affect MAPK signaling, a pathway that has been implicated in invadopodia formation in human melanoma cells (Tague et al., 2004).

Pharmacological inhibition of p110α blocks invadopodia formation

To confirm that p110α is an essential regulator of invadopodia formation, the effect of selective inhibitors of class I PI3K isoforms was investigated. Cells were cultured on fluorescent gelatin-coated coverslips in the presence of PIK-75, TGX-221, or IC87114, which are selective inhibitors of p110α, β, and δ, respectively (Knight et al., 2006; Chaussade et al., 2007). p110α inhibition by PIK-75 treatment significantly inhibited gelatin degradation in a dose-dependent manner, showing an IC_{50} of 25.0 nM (Fig. 3, A–C), and suppressed invadopodia formation (Fig. 3, D and E). A similar inhibition of gelatin degradation was observed when BT-549 and Hs578T breast cancer cells were treated with PIK-75 (Fig. S4, H and I). However, neither TGX-221 nor IC87114 significantly affected gelatin degradation (Fig. 3, A and C) despite their use at concentrations well above the IC_{50} values reported previously (Chaussade et al., 2007). PIK-75 treatment also markedly inhibited Matrigel invasion of MDA-MB-231 cells (Fig. 3 F).

As expected, we found that only p110α inhibition by PIK-75 suppressed EGF-induced Akt phosphorylation (Fig. 3 G). In addition, EGF-induced phosphorylation of ERK was not affected by PIK-75 treatment (Fig. 3 G). At the concentrations used in these experiments, PIK-75 should specifically inhibit p110α activity but should not block p110β and p110δ activities based on results of previous studies (Knight et al., 2006; Chaussade et al., 2007). These results indicate that p110α plays a pivotal role in PI3K signaling and regulates the invadopodia-mediated ECM degradation activity of invasive breast cancer cells.

Downloaded from jcb.rupress.org on May 17, 2012

Published June 27, 2011

Activating mutations in the *PIK3CA* gene promote invadopodia formation

The *PIK3CA* gene, which encodes p110α, is one of the most frequently mutated genes in human breast cancers, and mutations in this gene are associated with invasion and metastasis (Saal et al., 2005; Maruyama et al., 2007). Most of the mutations occur at two hot spots, namely E545K in the helical domain and H1047R in the catalytic domain. These mutations constitutively activate the PI3K signaling pathway (Isakoff et al., 2005; Kang et al., 2005). Accordingly, the effect of these *PIK3CA* mutations on invadopodia formation was investigated in MDA-MB-231 cells, which express wild-type (WT) p110α (Hollestelle et al., 2007). MDA-MB-231 cell lines stably expressing WT, E545K, or H1047R p110α were generated. The expression levels of the ectopic proteins were ~4–5 times higher than the expression level of the endogenous protein (Fig. 4 A). The results showed an increase in EGF-induced Akt phosphorylation in cells expressing WT p110α and a further increase in cells expressing either E545K or H1047R p110α in comparison to control mock-infected cells (Fig. 4 B). Furthermore, morphological analysis revealed that WT p110α cells tended to form more lamellipodia or membrane ruffles than control mock-infected cells (Fig. 4 C). An additional increase in the protrusive activities in E545K- and H1047R-expressing cells was observed (Fig. 4 C), which may reflect enhanced cell motility induced by these p110α mutants as described previously (Pang et al., 2009). Invadopodia formation and gelatin degradation activity were moderately increased in WT p110α cells and further enhanced in E545K- and H1047R-expressing cells (Fig. 4, D–G). The enhanced gelatin degradation activity in E545K- and H1047R-expressing cells was still sensitive to PIK-75 treatment, indicating that the enzymatic activity is crucial for invadopodia formation (Fig. 4 H). Similar to the behavior of the endogenous protein, the E545K and H1047R p110α mutants also accumulated at gelatin degradation sites (Fig. 4 I). In addition, E545K- and H1047R-expressing cells showed enhanced invasion through Matrigel compared with mock-infected cells (Fig. 4 J). These findings indicate that these activating mutations in the *PIK3CA* gene commonly present in human cancers promote the invadopodia-mediated invasive activity of breast cancer cells.

PDK1 and Akt are involved in invadopodia formation

To determine the downstream target of p110α associated with invadopodia formation, the role of PDK1 was examined. PDK1 has been shown to translocate to the plasma membrane upon activation of PI3Ks, and phosphorylate downstream targets, including Akt (Toker and Newton, 2000). PDK1 expression in MDA-MB-231 cells was confirmed by immunoblotting and suppressed by two different siRNA sequences that target different regions of the *PDK1* gene (Fig. 5 A). PDK1 down-regulation clearly impaired invadopodia formation in these cells and the related gelatin matrix degradation (Fig. 5, B–D).

The role of Akt in invadopodia formation was then examined. The expression of all Akt isoforms (i.e., Akt1, Akt2, and Akt3) was detected in MDA-MB-231 cells by real-time quantitative PCR (Fig. S3 B). To avoid possible functional redundancy, all Akt isoforms were simultaneously knocked down. In cells transfected with two different sets of siRNAs, the expression of total Akt was efficiently suppressed (Fig. 5 E). Akt knockdown significantly decreased invadopodia formation and gelatin degradation (Fig. 5, F–H). Furthermore, knockdown of PDK1 or Akt markedly decreased invadopodia formation in both E545K and H1047R p110α cells (Fig. 5 I). Examination of the localization of endogenous Akt and PDK1 proteins revealed that these proteins accumulated at invadopodia-mediated gelatin degradation sites in MDA-MB-231 cells (Fig. 5 J) and BT549 cells (Fig. S4 J). These results indicate that the role of PDK1 and Akt as downstream targets of p110α is essential for invadopodia formation.

Pharmacological inhibition of PDK1 and Akt blocks invadopodia formation

To further confirm the involvement of PDK1 and Akt, cells were treated with OSU-03012 and the Akt inhibitor VIII, which are inhibitors of PDK1 and Akt, respectively. Although its specificity may need better characterization, OSU-03012 was shown to potently inhibit PDK1 activity by competing with ATP (Zhu et al., 2004). The Akt inhibitor VIII is a PH domain–dependent specific Akt inhibitor and blocks activation of Akt (Barnett et al., 2005). Treatment of cells with these inhibitors resulted in a decrease in the levels of phosphorylated Akt (Fig. 6, A and B). These inhibitors markedly blocked gelatin degradation activity (IC_{50} = 3.9 μM for OSU-03012 and 2.2 μM for Akt inhibitor VIII; Fig. 6, C–F) and invadopodia formation (Fig. 6, G–J). We also examined the effect of a PKC inhibitor on invadopodia formation because PKC is another major substrate of PDK1 (Toker and Newton, 2000). When treated with the broad-range PKC inhibitors calphostin and GF109203X, MDA-MB-231 cells showed no obvious changes in gelatin degradation activity (Fig. 6 C). Moreover, OSU-03012 and the Akt inhibitor VIII significantly blocked gelatin degradation activities of cells expressing the activating mutants of p110α (Fig. 6 K).

Overexpression of Akt constructs affects invadopodia formation

The effect of the ectopic expression of various Akt constructs was examined by generating MDA-MB-231 cell lines stably expressing WT, kinase dead (KD), or a membrane-targeted constitutively active form (myristoylated [Myr]) of Akt1. Akt phosphorylation increased in cells expressing WT Akt1 but decreased in cells expressing KD Akt1 in comparison to control mock-infected cells (Fig. 7 A). Myr Akt1 expression robustly enhanced Akt phosphorylation (Fig. 7 A). Invadopodia formation and gelatin degradation activity were increased in WT Akt1 cells but decreased in KD Akt1 cells, which is consistent with the changes in Akt phosphorylation (Fig. 7, B–E). Unexpectedly, however, cells expressing Myr Akt1 showed a marked decrease in invadopodia formation and gelatin degradation (Fig. 7, B–E). Ectopically expressed WT Akt1 accumulated at invadopodia in a similar manner to endogenous protein (Fig. 7 F).

Downloaded from jcb.rupress.org on May 17, 2012

Published June 27, 2011

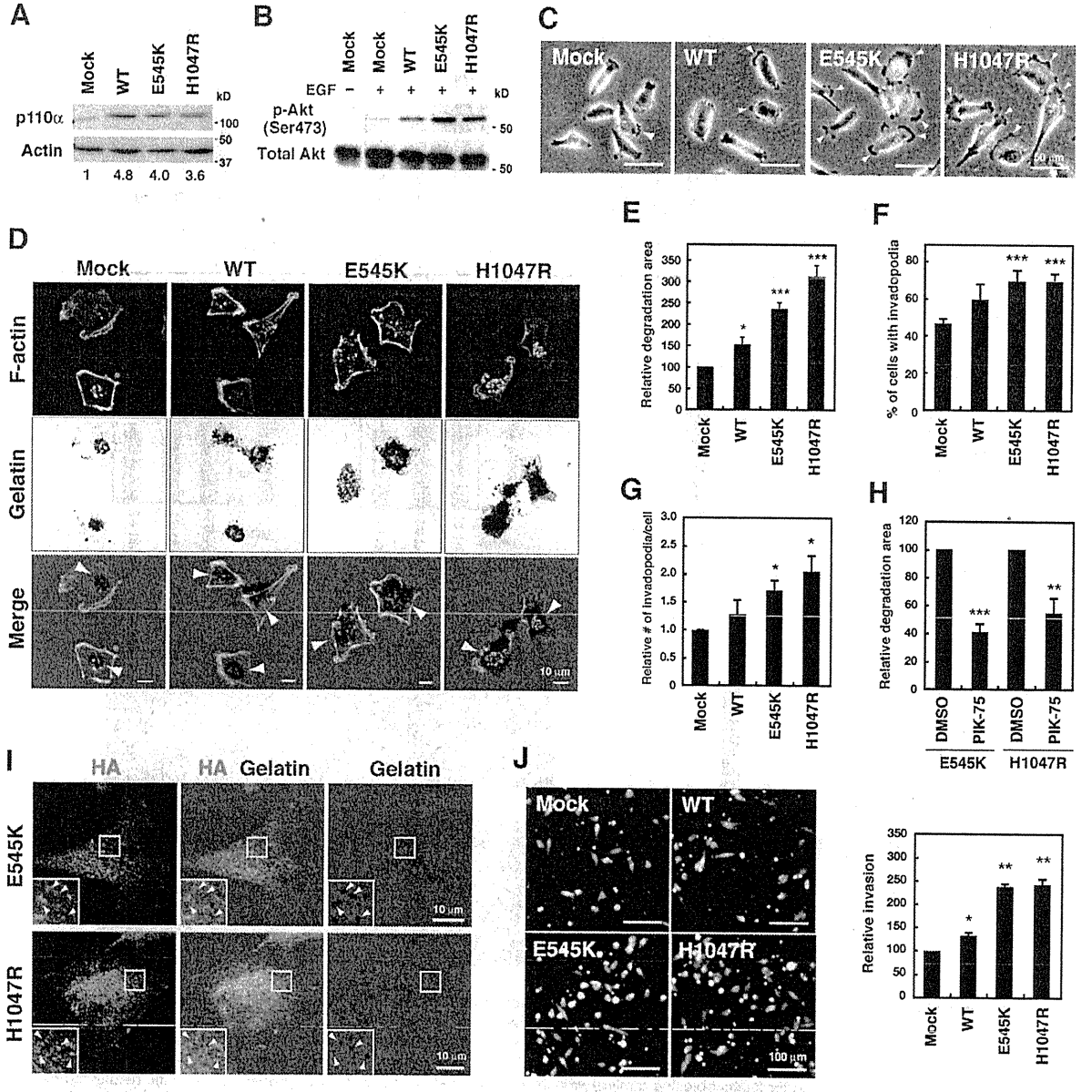

Figure 4. **Cancerous p110α mutations promote invadopodia formation.** (A) MDA-MB-231 cells stably expressing wild-type (WT), E545K, or H1047R p110α were analyzed by immunoblotting. Numbers below represent relative expression levels of the p110α constructs. (B) Cell lines stably expressing p110α were serum-starved overnight and stimulated with 8 nM EGF for 10 min. The phosphorylation status of Akt (p-Akt) was determined by immunoblotting. (C) Phase-contrast images show the morphology of the p110α cell lines. Arrowheads denote membrane protrusions. (D) Cells stably expressing the p110α constructs were cultured on fluorescent gelatin matrices for 7 h and stained with phalloidin to visualize invadopodia. Arrowheads denote the gelatin degradation sites. (E–G) Gelatin degradation activity (E), the percentage of cells with invadopodia (F), and the number of invadopodia per cell (G) were determined in p110α cell lines. (H) Cells expressing E545K or H1047R p110α were examined for gelatin degradation in the presence or absence of 100 nM PIK-75. (I) Cells expressing E545K or H1047R p110α were cultured on fluorescent gelatin matrices for 4 h and stained with anti-HA antibody to visualize localization of E545K and H1047R p110α. Insets are magnified images of the boxed regions. Arrowheads denote colocalization of the HA signals with the gelatin degradation sites. (J) Cells labeled with CellTracker green were analyzed for invasion through Matrigel-coated Transwell inserts for 24 h. Data are represented as means + SEM of seven (E), six (F–H), and three (J) independent determinations. *, $P < 0.05$; **, $P < 0.01$; and ***, $P < 0.001$ by Student's *t* tests.

In contrast, Myr Akt1 uniformly distributed throughout the plasma membrane and showed no specific localization (Fig. 7 F). We also generated MDA-MB-231 cell lines expressing other constitutively active forms of Akt1, namely E17K and E40K, which have a higher affinity for phosphoinositides (Aoki et al., 1998; Carpten et al., 2007). Although the expression of these Akt1 mutants markedly increased Akt phosphorylation, it abrogated invadopodia-mediated gelatin degradation activity (Fig. S5, A and B). Collectively, these results confirm the role of Akt in invadopodia formation and suggest that site-specific and proper activation of Akt is necessary for efficient assembly of invadopodia.

Downloaded from jcb.rupress.org on May 17, 2012

Published June 27, 2011

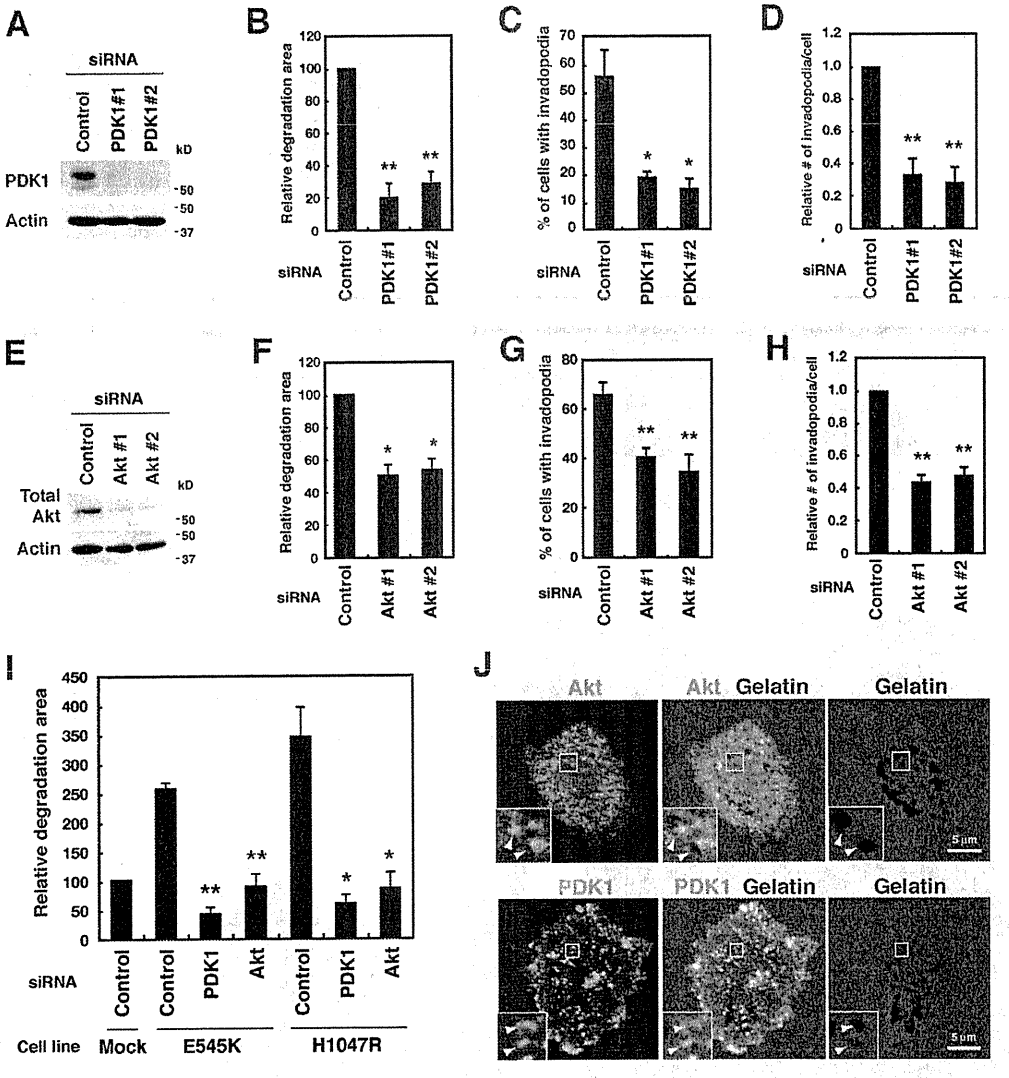

Figure 5. **PDK1 and Akt are essential downstream effectors of p110α for invadopodia formation.** (A) MDA-MB-231 cells were transfected with control or two distinct PDK1 siRNAs for 48 h and used for immunoblotting to determine the amount of PDK1. (B–D) Cells transfected with the control or PDK1 siRNA were cultured on fluorescent gelatin-coated coverslips for 7 h. Degraded areas on the gelatin matrix (B), the percentage of cells with invadopodia (C), and the number of invadopodia per cell (D) were quantified for transfected cells. (E) Cells were transfected with control or two different sets of siRNAs targeting Akt1, 2, and 3 for 48 h and used for immunoblotting analysis with the anti–pan-Akt antibody. (F–H) Degraded areas on the gelatin matrix (F), the percentage of cells with invadopodia (G), and the number of invadopodia per cell (H) were quantified for siRNA-transfected cells. (I) Cells stably expressing E545K or H1047R p110α were transfected with indicated siRNAs for 48 h and tested for invadopodia activities for 7 h. (J) MDA-MB-231 cells plated onto fluorescent gelatin-coated coverslips for 4 h were stained with the anti-Akt or anti-PDK1 antibody. Insets are magnified images of the boxed regions. Arrowheads denote the accumulation of Akt and PDK1 signals at the gelatin degradation sites. Data are represented as means + SEM of six (B, G, and H), four (C, D, and I), and three (F) independent determinations. *, $P < 0.02$; and **, $P < 0.005$ by Student's *t* tests.

Discussion

In the present study, the PI3K inhibitors LY294002 and wortmannin were shown to effectively inhibit invadopodia formation in MDA-MB-231 human breast cancer cells. This result is consistent with the previous studies describing that the formation of invadopodia in human cancer cells and podosomes in Src transformed fibroblasts requires the activity of PI3K (Nakahara et al., 2003; Mandal et al., 2008; Oikawa et al., 2008).

Overexpression of the Akt-PH domain, which sequesters the PI3K products $PI(3,4,5)P_3$ and $PI(3,4)P_2$, effectively blocked invadopodia formation. Although the predominant product of PI3K is $PI(3,4,5)P_3$, several evidence raise the possibility that $PI(3,4)P_2$ also plays a significant and redundant role in invadopodia formation in parallel with $PI(3,4,5)P_3$ (Fig. 8). Chuang et al. (2004) reported that siRNA knockdown of synaptojanin-2, which generates $PI(3,4)P_2$ via dephosphorylation of $PI(3,4,5)P_3$, blocks invadopodia formation in glioma cells. Moreover, Oikawa et al. (2008) reported that $PI(3,4)P_2$ regulates podosome formation by recruiting Tks5 and N-WASP, which are essential components of podosomes. Therefore, although further studies are required to precisely define the individual roles of $PI(3,4,5)P_3$ and $PI(3,4)P_2$, our results indicate that these D3-phosphoinositides

Downloaded from jcb.rupress.org on May 17, 2012

Published June 27, 2011

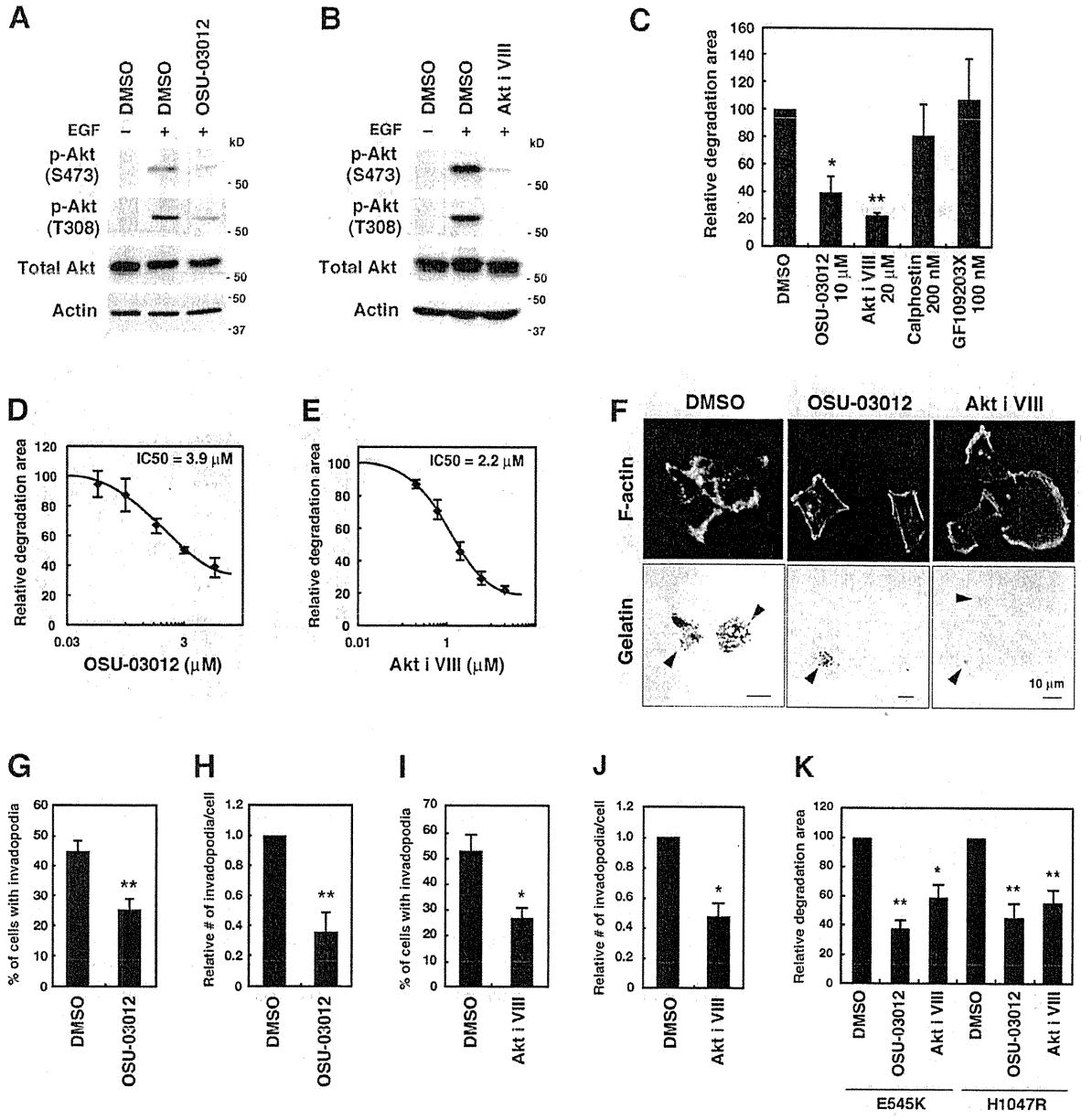

Figure 6. **Pharmacological inhibition of PDK1 and Akt blocks invadopodia formation.** (A and B) MDA-MB-231 cells were serum-starved overnight and treated with inhibitors, 10 μM OSU-03012 for PDK1 (A) or 20 μM Akt inhibitor VIII (Akt i VIII) for Akt (B) for 1 h. The cells were subsequently stimulated with 8 nM EGF for 10 min and used for immunoblotting to determine the phosphorylation status of Akt (p-Akt). (C) MDA-MB-231 cells were cultured on fluorescent gelatin-coated coverslips for 7 h in the presence of various inhibitors, including OSU-03012, Akt inhibitor VIII, and calphostin, and GF109203X for PKC. The degraded areas on the gelatin matrix were quantified. (D and E) Dose–response curves of gelatin degradation obtained in the presence of increasing concentrations of OSU-03012 (D) or Akt inhibitor VIII (E) are shown. (F) Representative images of MDA-MB-231 cells treated with 10 μM OSU-03012 and 20 μM Akt inhibitor VIII are shown. Arrowheads denote the gelatin degradation sites. (G–J) The percentage of cells with invadopodia (G and I) and the relative number of invadopodia per cell (H and J) were quantified for cells treated with 10 μM OSU-03012 (G and H) or 20 μM Akt inhibitor VIII (I and J). (K) Cells expressing E545K or H1047R p110α were examined for gelatin degradation in the presence of 10 μM OSU-03012 or 20 μM Akt inhibitor VIII. Data are represented as means ± SEM of six (C, I, and J), four (E, G, H, and K), and three (D) independent determinations. *, $P < 0.02$; and **, $P < 0.005$ by Student's *t* tests.

produced by PI3K activity play an essential role in invadopodia biogenesis.

We and other researchers have previously reported that invadopodia formation is initiated with the assembly of actin core structures followed by the accumulation of matrix metalloproteinases for ECM degradation (Yamaguchi et al., 2005a; Artym et al., 2006; Oser et al., 2009). The finding that treatment of cells with PI3K inhibitors blocked the formation of F-actin and cortactin structures of invadopodia suggests that PI3K signaling is involved in the first step of invadopodia formation. In support of this hypothesis, PI3K inhibitors disassembled the F-actin structures of invadopodia, as shown by time-lapse analysis, and

Downloaded from jcb.rupress.org on May 17, 2012

Published June 27, 2011

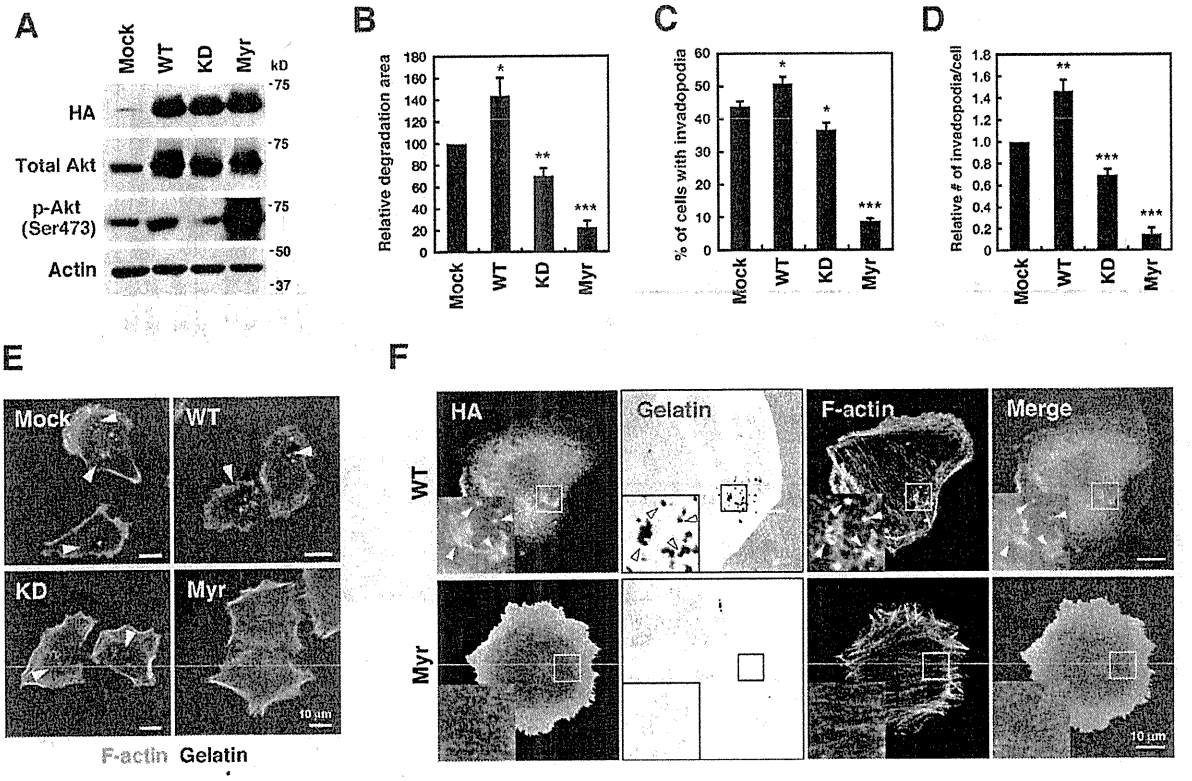

Figure 7. **Expression of Akt constructs affects invadopodia formation.** (A) MDA-MB-231 cells stably expressing HA-tagged wild-type (WT), kinase-dead (KD), or myristoylated constitutively active (Myr) Akt1 were analyzed by immunoblotting. (B–D) Cells stably expressing the Akt constructs were cultured on fluorescent gelatin-coated coverslips for 7 h and stained for F-actin. Degraded areas on the gelatin matrix (B), the percentage of cells with invadopodia (C), and the number of invadopodia per cell (D) were quantified. Data are represented as means + SEM of six (B) and four to eight (C and D) independent determinations. *, $P < 0.05$; **, $P < 0.01$; and ***, $P < 0.001$ by Student's *t* tests. (E) Representative images of cells expressing the Akt constructs. Arrowheads denote the gelatin degradation sites. (F) Cells expressing WT or Myr Akt1 were cultured on fluorescent gelatin matrices for 3 h and stained with anti-HA antibody and phalloidin. Insets are magnified images of the boxed regions. Arrowheads denote localization of the HA signals at invadopodia.

that PI3K products were enriched with F-actin at the invadopodia, as detected with the GFP-Akt PH construct. Consistent with these observations, Mandal et al. (2008) recently reported that PI3K is required for the formation of F-actin cores of invadopodia induced by TGF-β stimulation.

An important finding of the present study was that among the PI3K isoforms, the class I PI3K catalytic subunit p110α is specifically involved in invadopodia formation. We showed that pharmacological inhibition of p110α blocked invadopodia-mediated ECM degradation and invasion in human breast cancer cell lines. Several inhibitors that target PI3Ks are currently being tested in clinical trials for the treatment of human cancers (Engelman, 2009). However, these broad-spectrum PI3K inhibitors can cause significant side effects caused by the multiple roles of the PI3K signaling pathway in basic cellular functions. Therefore, current research is extensively focused both on understanding the isoform-specific functions of PI3Ks and on developing isoform-specific inhibitors of the PI3K family proteins (Zhao and Vogt, 2008; Engelman, 2009; Jia et al., 2009).

Recent studies have delineated distinct functions of class I PI3K isoforms (Engelman, 2009; Jia et al., 2009). The p110α subunit was shown to predominantly mediate PI3K signaling activity in receptor tyrosine kinase signal transduction, whereas p110β responds to G protein–coupled receptors (Zhao et al., 2006; Guillermet-Guibert et al., 2008). In addition, it has been reported that immune system function is largely dependent on p110δ and p110γ (Rommel et al., 2007). Moreover, unlike *PIK3CA*, which encodes p110α, cancer-specific mutations have not been reported for genes encoding other class I PI3Ks (Jia et al., 2009). Based on these findings and the specific role of p110α in invadopodia formation, we hypothesize that p110α is a promising therapeutic target for the treatment of cancer invasion and metastasis with minimal side effects.

The *PIK3CA* mutations found in human cancers primarily occur at two hot spots: E545K in the helical domain and H1047R in the catalytic domain (Samuels and Ericson, 2006; Zhao and Vogt, 2008). These mutations are known to promote the catalytic activity of p110α, thereby leading to constitutive activation of the PI3K signaling pathway (Kang et al., 2005). We determined that the E545K and H1047R mutations in p110α enhanced invadopodia-mediated ECM degradation and invasion. This finding provides mechanistic insight into the role of p110α mutations in cancer invasion.

Although we clearly showed that basal p110α activity is required for invadopodia formation, mutations of p110α are not sufficient to trigger invadopodia formation. In fact, several breast cancer cell lines that contain p110α mutations, such as MCF-7 and T47D (Hollestelle et al., 2007), are unable to form

Downloaded from jcb.rupress.org on May 17, 2012

Published June 27, 2011

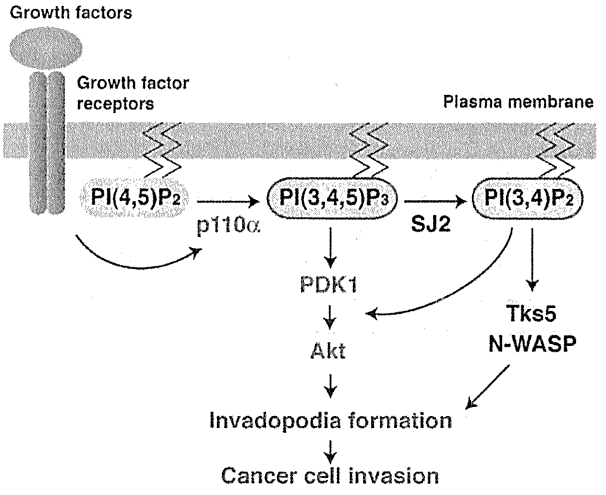

Figure 8. **A model of the function of PI3K signaling in invadopodia formation and cell invasion.** p110α that is activated downstream of growth factor receptors produces the signaling lipid $PI(3,4,5)P_3$ to regulate invadopodia formation and cancer cell invasion. $PI(3,4)P_2$ that is generated via dephosphorylation of $PI(3,4,5)P_3$ by synaptojanin-2 (SJ2) may regulate invadopodia formation through the Tks5/N-WASP axis in parallel with $PI(3,4,5)P_3$. PDK1 and Akt are activated by both $PI(3,4,5)P_3$ and $PI(3,4)P_2$ and act as mediators of the PI3K signaling pathway for invadopodia formation.

invadopodia as reported previously (Coopman et al., 1998; Yamaguchi et al., 2009). Therefore, it is likely that activation of other factors and/or signaling pathways trigger invadopodia formation, and the concurrent activation of p110α by mutations may act as a positive modulator in this process. This concept is supported by the fact that activating p110α mutations are preferentially observed in invasive tumors (Saal et al., 2005; Maruyama et al., 2007) and often associated with other alterations, such as ERBB2 overexpression and *K-ras* mutations (Oda et al., 2008).

In the present study, we demonstrated, for the first time, that PDK1 and Akt are involved in invadopodia formation. Importantly, knockdown and pharmacological inhibition of Akt or PDK1 abolished the enhanced invadopodia formation induced by E545K and H1047R p110α. Previous studies have shown that PDK1 and Akt are overexpressed and/or mutated in various human cancers and have implicated these proteins in cancer invasion and metastasis (Xie et al., 2006; Pinner and Sahai, 2008; Liu et al., 2009; Sheng et al., 2009). Therefore, our findings may provide a further rationale for targeting PDK1 and Akt in addition to p110α in the development of antiinvasion and antimetastasis strategies.

Additional evidence that Akt is required for invadopodia formation was provided by the overexpression of WT and KD forms of Akt. Unexpectedly, however, overexpression of constitutively active forms of Akt markedly blocked invadopodia formation. Because we observed that Akt localized to invadopodia, site-specific and controlled activation of Akt by p110α and PDK1 may be required for proper invadopodia formation and cancer invasion. In agreement with this idea, the constitutively active form of Akt was shown to inhibit the invasion of breast cancer cells both in vitro and in vivo (Hutchinson et al., 2004; Liu et al., 2006). Further studies are necessary to elucidate the exact mechanisms underlying the regulation of invadopodia formation by the p110α–PDK1–Akt pathway.

In conclusion, our results strongly suggest that the PI3K signaling pathway mediated by p110α is a critical regulator of invadopodia-mediated invasion of human breast cancer cells. These findings identified a new cellular function of the well-known oncogene product p110α and provided new insights into the molecular mechanisms of invadopodia formation and cancer cell invasion.

Materials and methods

Cell culture

Human breast cancer cell lines MDA-MB-231, BT-549, and Hs578T were obtained from the American Type Culture Collection. MDA-MB-231 cells were maintained in a 1:1 mixture of high glucose-DME and RPMI 1640 supplemented with 10% FBS, 10 U/ml penicillin, and 10 µg/ml streptomycin. BT-549 and Hs578T cells were maintained in RPMI 1640 and DME, respectively, supplemented as described previously in this paragraph.

Antibodies, reagents, and constructs

Alexa dyes, fluorescently labeled phalloidin, and secondary antibodies were purchased from Invitrogen. LY294002, wortmannin, anti-p110α, anti-p110β, anti-ERK, and anti-Akt antibodies were purchased from Cell Signaling Technology. The anti-p110δ antibody, calphostin, and Akt inhibitor VIII were purchased from EMD. Recombinant human EGF was purchased from Millipore. The anti-HA antibody was purchased from Covance. PIK-75 and IC87114 were purchased from Symansis. TGX-221 was purchased from Cayman Chemical. OSU-03012 was purchased from Echelon Biosciences. GF109203X was purchased from Enzo Life Sciences. The anti–β-actin antibody, gelatin, and other chemicals were purchased from Sigma-Aldrich. For GFP-Akt-PH domain constructs, the cDNA that encoded the mouse Akt-PH domain (1–111 aa) was subcloned into the pEGFP-C1 vector (Takara Bio Inc.). pBabe-puro constructs for HA-tagged WT, E545K, and H1047R forms of p110α were provided by J. Zhao (Harvard Medical School, Boston, MA; Zhao et al., 2005) through Addgene. pLNCX constructs for HA-tagged WT, KD, and constitutively active Myr forms of Akt were provided by W. Sellers (Harvard Medical School, Boston, MA; Ramaswamy et al., 1999) through Addgene. The mutagenesis basal kit (PrimeSTAR; Takara Bio Inc.) and site-directed mutagenesis kit (QuickChange Lightning; Agilent Technologies) were used to generate the Akt-PH domain R25C mutant and Akt1 E17K and E40K mutants.

Plasmid transfection, retroviral infection, lentiviral infection, and generation of stable cell lines

MDA-MB-231 cells were transfected with the indicated plasmids using Lipofectamine 2000 (Invitrogen) or Lipofectamine LTX (Invitrogen) according to the manufacturer's instructions. To generate stable cell lines, transfected cells were selected with G418 at 1 mg/ml, and resistant clones were isolated. For retroviral infection, cDNAs were inserted into the pMXs-IP or pLNCX vector, and recombinant retroviruses were produced with the Platinum-A packaging cell line as previously described (Kitamura et al., 2003). In brief, Platinum-A cells were transfected with the retroviral constructs using Lipofectamine 2000, and the medium was changed at 1 d after transfection. Culture medium containing recombinant retroviruses was collected at 2 d after transfection and filtered through a 0.45-µm filter. Cells were immediately infected with the recombinant retroviruses in the presence of 5 µg/ml polybrene for 1 d and then selected with 1 µg/ml puromycin or 1 mg/ml G418. Control and p110α shRNA lentiviral particles were purchased from Santa Cruz Biotechnology, Inc. Lentiviral infection was performed according to the manufacturer's instructions, and infected cells were selected with 1 µg/ml puromycin.

Immunofluorescence analysis

Cells were fixed in 4% paraformaldehyde for 15 min and permeabilized with 0.1% Triton X-100 for 5 min. To detect the localization of GFP-Akt PH construct and PDK1, cells were fixed and permeabilized in 4% paraformaldehyde, 0.1% glutaraldehyde, and 0.075 mg/ml saponin for 1 h at 37°C. The cells were blocked in 1% BSA and 1% goat serum for 30 min. The cells were incubated with primary antibodies for 1 h and then

Downloaded from jcb.rupress.org on May 17, 2012

Published June 27, 2011

with fluorophore-conjugated secondary antibodies and phalloidin (Invitrogen) for 30 min. Samples were observed with a confocal microscope (IX81-ZDC-DSU; Olympus) equipped with a cooled charge-coupled device camera (ORCA-ER; Hamamatsu Photonics), and the imaging system was driven by MetaMorph software (Universal Imaging). All images were acquired using 60× (PLAPON60xO; NA 1.42) or 100× (UPLSAPO100xO; NA 1.4) oil objectives. Images were analyzed and processed with various software packages, including MetaMorph, ImageJ (version 1.41o; National Institutes of Health), and Photoshop (CS4; Adobe).

Time-lapse microscopic analysis

In brief, time-lapse series of cells were taken at 37°C using the aforementioned microscope (IX81-ZDC-DSU) equipped with a humidified CO_2 chamber. Digital images were converted in ImageJ 1.41o, and the fluorescence intensity of GFP-actin at the invadopodia was calculated.

RNAi

All RNAi experiments were performed using Stealth RNAi molecules (Invitrogen). The Stealth RNAi molecules used in this study are shown in Table S1. Cells were transfected with 30 nM siRNA using Lipofectamine RNAiMAX (Invitrogen) according to the manufacturer's instructions. The cells were cultured for 48–72 h and used for invadopodia formation assay and other assays.

RT-PCR

Total RNA was isolated with an RNeasy Plus Mini kit (QIAGEN). Template cDNAs were synthesized with SuperScript III (Invitrogen). Quantitative RT-PCR was performed with a quantitative PCR mix (THUNDERBIRD; TOYOBO) in a real-time PCR detection system (CFX96; Bio-Rad Laboratories). For standard PCR amplification, DNA polymerase (KOD-plus; TOYOBO) and PCR beads (puReTaq Ready-To-Go; GE Healthcare) were used. The sequences of primer pairs used in this study are shown in Table S2.

Immunoblotting

Cells were washed with ice-cold PBS twice before direct extraction in SDS-PAGE sample buffer or lysis in a buffer containing 25 mM Tris-HCl, pH 7.5, 150 mM NaCl, 2 mM EDTA, 1% NP-40, 1% sodium deoxycholate, 0.1% SDS, and a protease inhibitor cocktail (Roche). The samples were resolved by SDS-PAGE, transferred to polyvinylidene difluoride membranes, and blocked with 5% nonfat dried milk. The membranes were incubated first with primary antibodies for 1 h and then with peroxidase-conjugated secondary antibodies for 30 min. The antibodies were diluted in immunoreaction enhancer solution (Can Get Signal; TOYOBO). Immunoreactive bands were detected using an ECL-plus kit (GE Healthcare).

Invadopodia assay

Fluorescent matrix-coated dishes were prepared as previously described (Bowden et al., 2001). Gelatin was labeled with TRITC in a buffer containing 40 mM NaCl and 50 mM $Na_2B_4O_7$, pH 9.3, and unbound dyes were removed by extensive dialysis against PBS at 37°C. 12-mm circular coverslips were coated with 100 µl of 25-mg/ml fluorescent gelatin and 20-mg/ml sucrose in PBS and then cross-linked with 0.5% glutaraldehyde on ice for 15 min followed by 30 min at room temperature. After extensive washing with PBS, the coverslips were treated with 5 mg/ml sodium borohydrate for 5 min to quench autofluorescence of residual glutaraldehyde. The coverslips were then sterilized with 70% ethanol for 15 min. MDA-MB-231 cells were cultured on the gelatin-coated coverslips for 3–7 h. To quantitate the gelatin degradation activity of invadopodia, we calculated the degradation area observed in images with the ImageJ 1.41o software and normalized the measurements to the total number of cells in each image. 10 randomly selected fields, usually containing 30–50 cells in total, were imaged with a 60× objective and analyzed for each experiment. The values of control cells were set to 100%, and the relative values of other cells were then calculated accordingly. The relative number of invadopodia and the percentage of cells with invadopodia were also calculated from the microscopy images.

EGF stimulation

Cells were serum-starved overnight in medium containing 0.35% BSA and stimulated with 8 nM EGF for 10 min at 37°C. The cells were subsequently washed twice with ice-cold PBS and lysed with a lysis buffer containing 50 mM Tris-HCl, pH 7.5, 1% NP-40, 2 mM EDTA, 100 mM NaCl, 1 mM sodium orthovanadate, and a protease inhibitor cocktail. The lysates were separated from cell debris by centrifugation and used for immunoblotting.

Invasion assay

Matrigel invasion assay was performed with a tumor invasion system (BioCoat; BD) composed of 24-multiwell inserts plates (8-µm pore size; Falcon FluoroBlok; BD) coated with Matrigel matrix (BD). The insert wells were rehydrated with 500 µl PBS for 2 h at 37°C. Cells were labeled with green 5-chloromethylfluorescein diacetate (CellTracker; Invitrogen) and resuspended at 1×10^5/ml in serum-free medium. 500 µl of the labeled cell suspension was added to the upper chambers, and 750 µl of growth medium containing 10% FBS was added to the lower chambers as a chemoattractant. After 24 h of incubation at 37°C, cells that invaded onto the lower surface of the filters were directly imaged with a confocal microscope (IX81-ZDC-DSU) using a 10× objective (UPLFLN 10×2PH; NA 0.3). Invaded cells were counted in five randomly selected fields per filter, the mean number of control cells was set to 100%, and the relative values of other cells were then calculated in each experiment.

Statistical analysis

Data are representative of at least three independent experiments. Statistical analysis was performed using Student's *t* tests. All p-values shown are versus control cells.

Online supplemental material

Fig. S1 shows the effects of PI3K inhibitors LY294002 and Wortmannin on invadopodia formation. Fig. S2 shows the expression levels of GFP-Akt-PH and the localization of GFP in MDA-MB-231 cells. Fig. S3 shows RT-PCR analysis of the expression of PI3K and Akt isoforms in MDA-MB-231 cells. Fig. S4 shows the effects of p110α knockdown and PIK-75 treatment on invadopodia formation and localization of PDK1 and Akt at invadopodia in human breast cancer cell lines. Fig. S5 shows the effects of the expression of E17K and E40K Akt1 constructs on invadopodia formation. Table S1 and Table S2 show siRNA and primer sequences, respectively, used in this study. Video 1 and Video 2 show disassembly of invadopodia by LY294002 treatment in MDA-MB-231 cells expressing GFP-actin and Venus-cortactin, respectively. Online supplemental material is available at http://www.jcb.org/cgi/content/full/jcb.201009126/DC1.

We are grateful to Drs. J. Zhao and W. Sellers for kindly providing plasmids. We thank Yumiko Konko and Keiko Takayama for their technical assistance.

This work was supported by Grants-in-Aid for Scientific Research (B), for Young Scientists (B), and for Cancer Research from the Ministry of Education, Culture, Sports, Science and Technology of Japan and by a Grant-in-Aid from the Ministry of Health, Labor and Welfare of Japan for the third term Comprehensive 10-Year Strategy for Cancer Control. This work was also supported in part by the Mochida Memorial Foundation for Medical and Pharmaceutical Research, the Ono Medical Research Foundation, and the Takeda Science Foundation.

Submitted: 27 September 2010
Accepted: 31 May 2011

References

Aoki, M., O. Batista, A. Bellacosa, P. Tsichlis, and P.K. Vogt. 1998. The akt kinase: molecular determinants of oncogenicity. *Proc. Natl. Acad. Sci. USA.* 95:14950–14955. doi:10.1073/pnas.95.25.14950

Artym, V.V., Y. Zhang, F. Seillier-Moiseiwitsch, K.M. Yamada, and S.C. Mueller. 2006. Dynamic interactions of cortactin and membrane type 1 matrix metalloproteinase at invadopodia: defining the stages of invadopodia formation and function. *Cancer Res.* 66:3034–3043. doi:10.1158/0008-5472.CAN-05-2177

Barnett, S.F., D. Defeo-Jones, S. Fu, P.J. Hancock, K.M. Haskell, R.E. Jones, J.A. Kahana, A.M. Kral, K. Leander, L.L. Lee, et al. 2005. Identification and characterization of pleckstrin-homology-domain-dependent and isoenzyme-specific Akt inhibitors. *Biochem. J.* 385:399–408. doi:10.1042/BJ20041140

Bowden, E.T., P.J. Coopman, and S.C. Mueller. 2001. Invadopodia: unique methods for measurement of extracellular matrix degradation in vitro. *Methods Cell Biol.* 63:613–627. doi:10.1016/S0091-679X(01)63033-4

Buccione, R., G. Caldieri, and I. Ayala. 2009. Invadopodia: specialized tumor cell structures for the focal degradation of the extracellular matrix. *Cancer Metastasis Rev.* 28:137–149. doi:10.1007/s10555-008-9176-1

Cain, R.J., and A.J. Ridley. 2009. Phosphoinositide 3-kinases in cell migration. *Biol. Cell.* 101:13–29. doi:10.1042/BC20080079

Caldieri, G., and R. Buccione. 2010. Aiming for invadopodia: organizing polarized delivery at sites of invasion. *Trends Cell Biol.* 20:64–70. doi:10.1016/j.tcb.2009.10.006

Downloaded from jcb.rupress.org on May 17, 2012

Published June 27, 2011

Cantley, L.C. 2002. The phosphoinositide 3-kinase pathway. *Science*. 296:1655–1657. doi:10.1126/science.296.5573.1655

Carpten, J.D., A.L. Faber, C. Horn, G.P. Donoho, S.L. Briggs, C.M. Robbins, G. Hostetter, S. Boguslawski, T.Y. Moses, S. Savage, et al. 2007. A transforming mutation in the pleckstrin homology domain of AKT1 in cancer. *Nature*. 448:439–444. doi:10.1038/nature05933

Chaussade, C., G.W. Rewcastle, J.D. Kendall, W.A. Denny, K. Cho, L.M. Grønning, M.L. Chong, S.H. Anagnostou, S.P. Jackson, N. Daniele, and P.R. Shepherd. 2007. Evidence for functional redundancy of class IA PI3K isoforms in insulin signalling. *Biochem. J.* 404:449–458. doi:10.1042/BJ20070003

Chen, W.T. 1989. Proteolytic activity of specialized surface protrusions formed at rosette contact sites of transformed cells. *J. Exp. Zool.* 251:167–185. doi:10.1002/jez.1402510206

Chen, W.T., C.C. Lee, L. Goldstein, S. Bernier, C.H. Liu, C.Y. Lin, Y. Yeh, W.L. Monsky, T. Kelly, M. Dai, et al. 1994. Membrane proteases as potential diagnostic and therapeutic targets for breast malignancy. *Breast Cancer Res. Treat.* 31:217–226. doi:10.1007/BF00666155

Chuang, Y.Y., N.L. Tran, N. Rusk, M. Nakada, M.E. Berens, and M. Symons. 2004. Role of synaptojanin 2 in glioma cell migration and invasion. *Cancer Res.* 64:8271–8275. doi:10.1158/0008-5472.CAN-04-2097

Clark, E.S., A.S. Whigham, W.G. Yarbrough, and A.M. Weaver. 2007. Cortactin is an essential regulator of matrix metalloproteinase secretion and extracellular matrix degradation in invadopodia. *Cancer Res.* 67:4227–4235. doi:10.1158/0008-5472.CAN-06-3928

Condeelis, J., and J.E. Segall. 2003. Intravital imaging of cell movement in tumours. *Nat. Rev. Cancer*. 3:921–930. doi:10.1038/nrc1231

Coopman, P.J., M.T. Do, E.W. Thompson, and S.C. Mueller. 1998. Phagocytosis of cross-linked gelatin matrix by human breast carcinoma cells correlates with their invasive capacity. *Clin. Cancer Res.* 4:507–515.

Dillon, R.L., D.E. White, and W.J. Muller. 2007. The phosphatidyl inositol 3-kinase signaling network: implications for human breast cancer. *Oncogene*. 26:1338–1345. doi:10.1038/sj.onc.1210202

Eckert, M.A., T.M. Lwin, A.T. Chang, J. Kim, E. Danis, L. Ohno-Machado, and J. Yang. 2011. Twist1-induced invadopodia formation promotes tumor metastasis. *Cancer Cell*. 19:372–386. doi:10.1016/j.ccr.2011.01.036

Engelman, J.A. 2009. Targeting PI3K signalling in cancer: opportunities, challenges and limitations. *Nat. Rev. Cancer*. 9:550–562. doi:10.1038/nrc2664

Engelman, J.A., J. Luo, and L.C. Cantley. 2006. The evolution of phosphatidylinositol 3-kinases as regulators of growth and metabolism. *Nat. Rev. Genet.* 7:606–619. doi:10.1038/nrg1879

Fruman, D.A., R.E. Meyers, and L.C. Cantley. 1998. Phosphoinositide kinases. *Annu. Rev. Biochem.* 67:481–507. doi:10.1146/annurev.biochem.67.1.481

Gimona, M., R. Buccione, S.A. Courtneidge, and S. Linder. 2008. Assembly and biological role of podosomes and invadopodia. *Curr. Opin. Cell Biol.* 20:235–241. doi:10.1016/j.ceb.2008.01.005

Guillermet-Guibert, J., K. Bjorklof, A. Salpekar, C. Gonella, F. Ramadani, A. Bilancio, S. Meek, A.J. Smith, K. Okkenhaug, and B. Vanhaesebroeck. 2008. The p110beta isoform of phosphoinositide 3-kinase signals downstream of G protein-coupled receptors and is functionally redundant with p110gamma. *Proc. Natl. Acad. Sci. USA*. 105:8292–8297. doi:10.1073/pnas.0707761105

Hollestelle, A., F. Elstrodt, J.H. Nagel, W.W. Kallemeijn, and M. Schutte. 2007. Phosphatidylinositol-3-OH kinase or RAS pathway mutations in human breast cancer cell lines. *Mol. Cancer Res.* 5:195–201. doi:10.1158/1541-7786.MCR-06-0263

Hutchinson, J.N., J. Jin, R.D. Cardiff, J.R. Woodgett, and W.J. Muller. 2004. Activation of Akt-1 (PKB-alpha) can accelerate ErbB-2-mediated mammary tumorigenesis but suppresses tumor invasion. *Cancer Res.* 64:3171–3178. doi:10.1158/0008-5472.CAN-03-3465

Isakoff, S.J., J.A. Engelman, H.Y. Irie, J. Luo, S.M. Brachmann, R.V. Pearline, L.C. Cantley, and J.S. Brugge. 2005. Breast cancer-associated PIK3CA mutations are oncogenic in mammary epithelial cells. *Cancer Res.* 65:10992–11000. doi:10.1158/0008-5472.CAN-05-2612

Jia, S., T.M. Roberts, and J.J. Zhao. 2009. Should individual PI3 kinase isoforms be targeted in cancer? *Curr. Opin. Cell Biol.* 21:199–208. doi:10.1016/j.ceb.2008.12.007

Kang, S., A.G. Bader, and P.K. Vogt. 2005. Phosphatidylinositol 3-kinase mutations identified in human cancer are oncogenic. *Proc. Natl. Acad. Sci. USA*. 102:802–807. doi:10.1073/pnas.0408864102

Kessenbrock, K., V. Plaks, and Z. Werb. 2010. Matrix metalloproteinases: regulators of the tumor microenvironment. *Cell*. 141:52–67. doi:10.1016/j.cell.2010.03.015

Kitamura, T., Y. Koshino, F. Shibata, T. Oki, H. Nakajima, T. Nosaka, and H. Kumagai. 2003. Retrovirus-mediated gene transfer and expression cloning: powerful tools in functional genomics. *Exp. Hematol.* 31:1007–1014.

Knight, Z.A., B. Gonzalez, M.E. Feldman, E.R. Zunder, D.D. Goldenberg, O. Williams, R. Loewith, D. Stokoe, A. Balla, B. Toth, et al. 2006. A pharmacological map of the PI3-K family defines a role for p110alpha in insulin signaling. *Cell*. 125:733–747. doi:10.1016/j.cell.2006.03.035

Li, S.Y., M. Rong, F. Grieu, and B. Iacopetta. 2006. PIK3CA mutations in breast cancer are associated with poor outcome. *Breast Cancer Res. Treat.* 96:91–95. doi:10.1007/s10549-005-9048-0

Linder, S. 2007. The matrix corroded: podosomes and invadopodia in extracellular matrix degradation. *Trends Cell Biol.* 17:107–117. doi:10.1016/j.tcb.2007.01.002

Liu, H., D.C. Radisky, C.M. Nelson, H. Zhang, J.E. Fata, R.A. Roth, and M.J. Bissell. 2006. Mechanism of Akt1 inhibition of breast cancer cell invasion reveals a protumorigenic role for TSC2. *Proc. Natl. Acad. Sci. USA*. 103:4134–4139. doi:10.1073/pnas.0511342103

Liu, Y., J. Wang, M. Wu, W. Wan, R. Sun, D. Yang, X. Sun, D. Ma, G. Ying, and N. Zhang. 2009. Down-regulation of 3-phosphoinositide-dependent protein kinase-1 levels inhibits migration and experimental metastasis of human breast cancer cells. *Mol. Cancer Res.* 7:944–954. doi:10.1158/1541-7786.MCR-08-0368

Madsen, C.D., and E. Sahai. 2010. Cancer dissemination—lessons from leukocytes. *Dev. Cell*. 19:13–26. doi:10.1016/j.devcel.2010.06.013

Mandal, S., K.R. Johnson, and M.J. Wheelock. 2008. TGF-beta induces formation of F-actin cores and matrix degradation in human breast cancer cells via distinct signaling pathways. *Exp. Cell Res.* 314:3478–3493. doi:10.1016/j.yexcr.2008.09.013

Maruyama, N., Y. Miyoshi, T. Taguchi, Y. Tamaki, M. Monden, and S. Noguchi. 2007. Clinicopathologic analysis of breast cancers with PIK3CA mutations in Japanese women. *Clin. Cancer Res.* 13:408–414. doi:10.1158/1078-0432.CCR-06-0267

Maurer, M., T. Su, L.H. Saal, S. Koujak, B.D. Hopkins, C.R. Barkley, J. Wu, S. Nandula, B. Dutta, Y. Xie, et al. 2009. 3-Phosphoinositide-dependent kinase 1 potentiates upstream lesions on the phosphatidylinositol 3-kinase pathway in breast carcinoma. *Cancer Res.* 69:6299–6306. doi:10.1158/0008-5472.CAN-09-0820

Nakahara, H., T. Otani, T. Sasaki, Y. Miura, Y. Takai, and M. Kogo. 2003. Involvement of Cdc42 and Rac small G proteins in invadopodia formation of RPMI7951 cells. *Genes Cells*. 8:1019–1027. doi:10.1111/j.1365-2443.2003.00695.x

Neve, R.M., K. Chin, J. Fridlyand, J. Yeh, F.L. Baehner, T. Fevr, L. Clark, N. Bayani, J.P. Coppe, F. Tong, et al. 2006. A collection of breast cancer cell lines for the study of functionally distinct cancer subtypes. *Cancer Cell*. 10:515–527. doi:10.1016/j.ccr.2006.10.008

Oda, K., J. Okada, L. Timmerman, P. Rodriguez-Viciana, D. Stokoe, K. Shoji, Y. Taketani, H. Kuramoto, Z.A. Knight, K.M. Shokat, and F. McCormick. 2008. PIK3CA cooperates with other phosphatidylinositol 3′-kinase pathway mutations to effect oncogenic transformation. *Cancer Res.* 68:8127–8136. doi:10.1158/0008-5472.CAN-08-0755

Oikawa, T., T. Itoh, and T. Takenawa. 2008. Sequential signals toward podosome formation in NIH-src cells. *J. Cell Biol.* 182:157–169. doi:10.1083/jcb.200801042

Oser, M., H. Yamaguchi, C.C. Mader, J.J. Bravo-Cordero, M. Arias, X. Chen, V. Desmarais, J. van Rheenen, A.J. Koleske, and J. Condeelis. 2009. Cortactin regulates cofilin and N-WASp activities to control the stages of invadopodium assembly and maturation. *J. Cell Biol.* 186:571–587. doi:10.1083/jcb.200812176

Pang, H., R. Flinn, A. Patsialou, J. Wyckoff, E.T. Roussos, H. Wu, M. Pozzuto, S. Goswami, J.S. Condeelis, A.R. Bresnick, et al. 2009. Differential enhancement of breast cancer cell motility and metastasis by helical and kinase domain mutations of class IA phosphoinositide 3-kinase. *Cancer Res.* 69:8868–8876. doi:10.1158/0008-5472.CAN-09-1968

Pinner, S., and E. Sahai. 2008. PDK1 regulates cancer cell motility by antagonising inhibition of ROCK1 by RhoE. *Nat. Cell Biol.* 10:127–137. doi:10.1038/ncb1675

Ramaswamy, S., N. Nakamura, F. Vazquez, D.B. Batt, S. Perera, T.M. Roberts, and W.R. Sellers. 1999. Regulation of G1 progression by the PTEN tumor suppressor protein is linked to inhibition of the phosphatidylinositol 3-kinase/Akt pathway. *Proc. Natl. Acad. Sci. USA*. 96:2110–2115. doi:10.1073/pnas.96.5.2110

Rommel, C., M. Camps, and H. Ji. 2007. PI3K delta and PI3K gamma: partners in crime in inflammation in rheumatoid arthritis and beyond? *Nat. Rev. Immunol.* 7:191–201. doi:10.1038/nri2036

Saal, L.H., K. Holm, M. Maurer, L. Memeo, T. Su, X. Wang, J.S. Yu, P.O. Malmström, M. Mansukhani, J. Enoksson, et al. 2005. PIK3CA mutations correlate with hormone receptors, node metastasis, and ERBB2, and are mutually exclusive with PTEN loss in human breast carcinoma. *Cancer Res.* 65:2554–2559. doi:10.1158/0008-5472-CAN-04-3913

Samuels, Y., and K. Ericson. 2006. Oncogenic PI3K and its role in cancer. *Curr. Opin. Oncol.* 18:77–82. doi:10.1097/01.cco.0000198021.99347.b9

Downloaded from jcb.rupress.org on May 17, 2012

Published June 27, 2011

Schoumacher, M., R.D. Goldman, D. Louvard, and D.M. Vignjevic. 2010. Actin, microtubules, and vimentin intermediate filaments cooperate for elongation of invadopodia. *J. Cell Biol.* 189:541–556. doi:10.1083/jcb.200909113

Sheng, S., M. Qiao, and A.B. Pardee. 2009. Metastasis and AKT activation. *J. Cell. Physiol.* 218:451–454. doi:10.1002/jcp.21616

Stephens, L., K. Anderson, D. Stokoe, H. Erdjument-Bromage, G.F. Painter, A.B. Holmes, P.R. Gaffney, C.B. Reese, F. McCormick, P. Tempst, et al. 1998. Protein kinase B kinases that mediate phosphatidylinositol 3,4,5-trisphosphate-dependent activation of protein kinase B. *Science.* 279:710–714. doi:10.1126/science.279.5351.710

Stylli, S.S., A.H. Kaye, and P. Lock. 2008. Invadopodia: at the cutting edge of tumour invasion. *J. Clin. Neurosci.* 15:725–737. doi:10.1016/j.jocn.2008.03.003

Tague, S.E., V. Muralidharan, and C. D'Souza-Schorey. 2004. ADP-ribosylation factor 6 regulates tumor cell invasion through the activation of the MEK/ERK signaling pathway. *Proc. Natl. Acad. Sci. USA.* 101:9671–9676. doi:10.1073/pnas.0403531101

Toker, A., and A.C. Newton. 2000. Cellular signaling: pivoting around PDK-1. *Cell.* 103:185–188. doi:10.1016/S0092-8674(00)00110-0

Várnai, P., T. Bondeva, P. Tamás, B. Tóth, L. Buday, L. Hunyady, and T. Balla. 2005. Selective cellular effects of overexpressed pleckstrin-homology domains that recognize PtdIns(3,4,5)P3 suggest their interaction with protein binding partners. *J. Cell Sci.* 118:4879–4888. doi:10.1242/jcs.02606

Weaver, A.M. 2006. Invadopodia: specialized cell structures for cancer invasion. *Clin. Exp. Metastasis.* 23:97–105. doi:10.1007/s10585-006-9014-1

Xie, Z., H. Yuan, Y. Yin, X. Zeng, R. Bai, and R.I. Glazer. 2006. 3-phosphoinositide-dependent protein kinase-1 (PDK1) promotes invasion and activation of matrix metalloproteinases. *BMC Cancer.* 6:77. doi:10.1186/1471-2407-6-77

Yamaguchi, H., M. Lorenz, S. Kempiak, C. Sarmiento, S. Coniglio, M. Symons, J. Segall, R. Eddy, H. Miki, T. Takenawa, and J. Condeelis. 2005a. Molecular mechanisms of invadopodium formation: the role of the N-WASP–Arp2/3 complex pathway and cofilin. *J. Cell Biol.* 168:441–452. doi:10.1083/jcb.200407076

Yamaguchi, H., J. Wyckoff, and J. Condeelis. 2005b. Cell migration in tumors. *Curr. Opin. Cell Biol.* 17:559–564. doi:10.1016/j.ceb.2005.08.002

Yamaguchi, H., Y. Takeo, S. Yoshida, Z. Kouchi, Y. Nakamura, and K. Fukami. 2009. Lipid rafts and caveolin-1 are required for invadopodia formation and extracellular matrix degradation by human breast cancer cells. *Cancer Res.* 69:8594–8602. doi:10.1158/0008-5472.CAN-09-2305

Yuan, T.L., and L.C. Cantley. 2008. PI3K pathway alterations in cancer: variations on a theme. *Oncogene.* 27:5497–5510. doi:10.1038/onc.2008.245

Zhao, J.J., Z. Liu, L. Wang, E. Shin, M.F. Loda, and T.M. Roberts. 2005. The oncogenic properties of mutant p110alpha and p110beta phosphatidylinositol 3-kinases in human mammary epithelial cells. *Proc. Natl. Acad. Sci. USA.* 102:18443–18448. doi:10.1073/pnas.0508988102

Zhao, J.J., H. Cheng, S. Jia, L. Wang, O.V. Gjoerup, A. Mikami, and T.M. Roberts. 2006. The p110alpha isoform of PI3K is essential for proper growth factor signaling and oncogenic transformation. *Proc. Natl. Acad. Sci. USA.* 103:16296–16300. doi:10.1073/pnas.0607899103

Zhao, L., and P.K. Vogt. 2008. Class I PI3K in oncogenic cellular transformation. *Oncogene.* 27:5486–5496. doi:10.1038/onc.2008.244

Zhu, J., J.W. Huang, P.H. Tseng, Y.T. Yang, J. Fowble, C.W. Shiau, Y.J. Shaw, S.K. Kulp, and C.S. Chen. 2004. From the cyclooxygenase-2 inhibitor celecoxib to a novel class of 3-phosphoinositide-dependent protein kinase-1 inhibitors. *Cancer Res.* 64:4309–4318. doi:10.1158/0008-5472.CAN-03-4063

Downloaded from jcb.rupress.org on May 17, 2012

Supplemental Material can be found at:
http://www.jbc.org/content/suppl/2011/03/28/M110.208587.DC1.html

THE JOURNAL OF BIOLOGICAL CHEMISTRY VOL. 286, NO. 20, pp. 18251–18260, May 20, 2011
© 2011 by The American Society for Biochemistry and Molecular Biology, Inc. Printed in the U.S.A.

Cancer Susceptibility Polymorphism of p53 at Codon 72 Affects Phosphorylation and Degradation of p53 Protein*[S]

Received for publication, December 14, 2010, and in revised form, March 18, 2011 Published, JBC Papers in Press, March 28, 2011, DOI 10.1074/jbc.M110.208587

Chikako Ozeki,[a,b,c] Yuichiro Sawai,[d,e] Tatsuhiro Shibata,[f] Takashi Kohno,[g] Koji Okamoto,[a,h] Jun Yokota,[g] Fumio Tashiro,[e] Sei-ichi Tanuma,[c] Ryuichi Sakai,[i] Tatsuya Kawase,[a,e] Issay Kitabayashi,[b] Yoichi Taya,[a,j1] and Rieko Ohki[a,d,i2]

From the [a]Radiobiology Division, [b]Molecular Oncology Division, [f]Division of Cancer Genomics, [g]Biology Division, [h]Early Oncogenesis Research Project, [i]Growth Factor Division, [d]Division of Cancer Biology, National Cancer Center Research Institute, Tsukiji 5-1-1, Chuo-ku, Tokyo 104-0045, Japan, the [e]Department of Biological Science and Technology, Faculty of Industrial Science and Technology, [c]Department of Biochemistry, Faculty of Pharmaceutical Sciences, Tokyo University of Science, Yamazaki 2641, Noda-shi, Chiba 270-8510, Japan, and the [j]Cancer Science Institute of Singapore and Department of Biochemistry, National University of Singapore, Center for Life Sciences 02-07, Medical Drive, 117456, Singapore

The common polymorphism of p53 at codon 72, either encoding proline or arginine, has drawn attention as a genetic factor associated with clinical outcome or cancer risk for the last 2 decades. We now show that these two polymorphic variants differ in protein structure, especially within the N-terminal region and, as a consequence, differ in post-translational modification at the N terminus. The arginine form (p53-72R) shows significantly enhanced phosphorylation at Ser-6 and Ser-20 compared with the proline form (p53-72P). We also show diminished Mdm2-mediated degradation of p53-72R compared with p53-72P, which is at least partly brought about by higher levels of phosphorylation at Ser-20 in p53-72R. Furthermore, enhanced p21 expression in p53-72R-expressing cells, which is dependent on phosphorylation at Ser-6, was demonstrated. Differential p21 expression between the variants was also observed upon activation of TGF-β signaling. Collectively, we demonstrate a novel molecular difference and simultaneously suggest a difference in the tumor-suppressing function of the variants.

The *p53* gene is a tumor suppressor gene, and loss of functional p53 is the most common anomaly found in human cancers (1). Signals activated upon various cellular stresses stabilize and activate p53, which exerts its tumor-suppressive function mainly by acting as a transcriptional activator. Target genes of p53 regulate a variety of processes, such as the induction of cell cycle arrest, cell death, DNA repair and senescence, and function downstream of p53 to prevent tumorigenesis (2). Depending on the stress signal, p53 selectively activates its target genes to implement various p53-mediated responses. Post-translational modification of p53 is a candidate mechanism that causes p53 to respond to different stress signals, and phosphorylation of p53 is the most major post-translational modification of p53 (3, 4). Kinases activated upon cellular stress, such as ataxia telangiectasia-mutated (ATM), ataxia telangiectasia and Rad3-related (ATR), and p38, phosphorylate serine and threonine residues, and phosphorylation results in the activation of p53 protein (5).

The structure of p53 protein is commonly divided into three functional domains as follows: the N-terminal domain, central core DNA-binding domain, and C-terminal domain. The N-terminal domain is required for the transcriptional activity of p53 protein and consists of two transactivation domains and a proline-rich domain. The transactivation domains are extensively phosphorylated upon p53 activation. Seven serines, Ser-6, -9, -15, -20, -33, -37, and -46, within the transactivation domain undergo phosphorylation (6). Phosphorylation of each residue has been reported to have specific physiological significance; for example, phosphorylation of Ser-15 or -46 modifies the transactivation ability of p53 (7–9), whereas Ser-20 is required for p53 protein stability (10). When not phosphorylated, p53 is actively degraded by the 26 S proteasome pathway by interacting with a ring finger ubiquitin E3 ligase, Mdm2. Upon activation, p53 is phosphorylated at Thr-18 and Ser-20, both of which reside within the Mdm2 binding domain, leading to reduced affinity with Mdm2 and escape from ubiquitination and subsequent degradation (11).

The proline-rich domain functions as a protein-protein interaction domain, and several proteins that bind to this region have been reported (12, 13). In particular, five P*XXP* motifs appearing in this domain are known to be critical for the interaction with Src homology 3 domain-containing proteins. In addition, within the proline-rich domain, a common polymorphism of p53 at codon 72, encoding either proline or arginine (p53-72P or p53-72R), has been reported (14–16). Notably, the proline at residue 72 of p53 is part of a P*XXP* motif, and

* This work was supported by grants-in-aid for scientific research from the Ministry of Education, Culture, Sports, Science, and Technology of Japan (to R. O., T. K., and Y. T.), grants-in-aid for the Third Term Comprehensive Ten-year Strategy for Cancer Control from the Ministry of Health, Labor, and Welfare Japan (to T. S., J. Y., and Y. T.), Program for Promotion of Fundamental Studies in Health Sciences of the National Institute of Biomedical Innovation (to T. S., T. K., and J. Y.), New Energy and Industrial Technology Development Organization (to R. O.), research grants from Hayashi Memorial Foundation for Female Natural Scientists (to R. O.), the Sagawa Foundation for Promoting Cancer Research (to R. O.), Takeda Science Foundation (to R. O.), Kobayashi Foundation for Cancer Research (to R. O.), and the Mochida Memorial Foundation for Medical and Pharmaceutical Research (to R. O.).

[S] The on-line version of this article (available at http://www.jbc.org) contains supplemental Figs. S1–S6.

[1] To whom correspondence may be addressed. E-mail: csiyt@nus.edu.sag.
[2] To whom correspondence may be addressed. Tel.: 81-3-3542-2511 (Ext. 4304); Fax: 81-3-3542-8170; E-mail: rohki@ncc.go.jp.

Downloaded from www.jbc.org at KOKURITSU GAN CENTER, on May 17, 2012

therefore it can be assumed that the polymorphism will affect protein-binding partners. Extensive studies have been carried out to investigate the link between the expression of p53 polymorphic variants at codon 72 and cancer susceptibility (17). It has been reported that in a number of cancers, including lung and breast, patients with the p53-72P allele are more susceptible to cancer development and a poor clinical outcome (18–21); however, the mechanistic basis for this bias is still an open question.

To determine the functional difference of the two variant proteins p53-72R and p53-72P, we first analyzed the protease accessibility of p53-72R and p53-72P, and we found that the higher order structures are different between them. We have also found that the phosphorylation modifications of both variants are different, leading to differential protein stability and transactivation ability of the two variants.

EXPERIMENTAL PROCEDURES

Plasmids—For p53 constructs, each p53 was cloned in pcDNA3 or pMX vector as described (22). When cloned in pMX vector, each p53 is under the control of a weak retroviral LTR promoter. Constitutively active TGF-β receptor I was constructed by introducing a point mutation at codon 204 (T204D) and cloned in pcDNA3. FLAG-tagged human wild-type Mdm2 (pSG-F-Hdm2), N-terminally c-Myc tagged Mdm2 (pCMV-Myc-Mdm2), and histidine-tagged ubiquitin expression plasmids were described previously (23).

Expression and Purification of Glutathione S-Transferase (GST) Fusion Proteins—GST fusion constructs of p53-72P and -72R were prepared by PCR tagging of p53 cDNA with BamHI and XhoI sites at the 5′ and 3′ ends, respectively, and subcloned into pGEX-6P-1 vector (Amersham Biosciences). Constructs were expressed in *Escherichia coli* (BL21-Gold (DE3) Competent Cell; Stratagene, CA) and purified from cell lysates using glutathione-Sepharose 4B beads (Amersham Biosciences). Purified proteins were further digested with PreScission protease (Amersham Biosciences) to cleave p53 from GST.

Cell Culture, Transfection, and Establishment of Stable Cell Lines—Cell culture was performed as described (22). Transient transfection assays were performed using Lipofectamine Plus or Lipofectamine 2000 reagent (Invitrogen), as indicated in the figure legends. Stable HCT116 p53(−/−) cell lines expressing p53-72P or -72R were obtained by infecting cells with recombinant retroviruses. In each case, as the control cell line, cells were also infected with empty retroviruses expressing only the drug resistance gene. Infection was performed in the presence of Polybrene (at 4 μg/ml; Sigma), and subsequently, cells were selected in puromycin (at 0.5 μg/ml; Sigma). To avoid possible disadvantages from utilizing clonal cell lines, *i.e.* clonal differences, cell lines were maintained as mass cultures.

Western Blotting Analysis and Immunoprecipitation—Cells were lysed in lysis buffer containing 50 mM Tris-HCl (pH 8.0), 1% Nonidet P-40, 250 mM NaCl, 50 mM NaF, 1 mM Na_3VO_4, 1 mM protease inhibitor (PMSF, aprotinin, and leupeptin), and 1 mM DDT. Whole cell lysates were subjected to protein quantification and subjected to immunoprecipitation or analyzed by Western blotting. The antibodies used in this study were as follows: anti-p53 goat polyclonal antibody (FL393); anti-p21 rabbit polyclonal antibody (C-19); anti-PIG3 (N-20) and PIG3 (C-20) goat polyclonal antibody; anti-Bax (N-20) mouse monoclonal antibody; anti-c-Myc mouse monoclonal antibody (9E10) and anti-β-actin mouse monoclonal antibody (Santa Cruz Biotechnology, Santa Cruz, CA); penta-His antibody (Qiagen, Valencia, CA); anti-p53 mouse monoclonal antibodies PAb1801 and PAb421 and anti-Mdm2 mouse monoclonal antibody (clone IF-2) (Calbiochem); anti-p53 mouse monoclonal antibody (PAb122) (Monosan, Uden, Netherlands); anti-phospho-p53 (Ser-6, -9, -15, -20, -37, and -46) rabbit polyclonal antibodies and anti-phospho-Smad2 (138D4) Ser-465/467 antibody (Cell Signaling, Beverly, MA); anti-CRP1 antibody (BD Transduction Laboratories); and anti-FLAG mouse monoclonal antibody (M2); and anti-tubulin antibody (clone B-5-1-2) (Sigma). To detect total p53, anti-p53 goat polyclonal antibody (FL393) was used in all cases.

Northern Blotting Analysis—RNA was prepared using an RNeasy Midi kit (Qiagen). Northern blotting was performed as described (22). Probes were prepared using a BcaBEST labeling kit (TaKaRa, Kyoto, Japan) and purified by serial purification using a Probe Quant G-50 MicroColumn (Amersham Biosciences) and NICK column (Amersham Biosciences). The full open reading frame of p53 was used for probe preparation.

Detection of Ubiquitinated p53—To detect efficiently the ubiquitinated p53, Mdm2 expression vector pSG-FLAG-Mdm2 was used, in which Mdm2 was expressed from an SV40 promoter (much weaker than CMV promoter). pcDNA3-p53-72P or -72R (0.35 μg), together with His_6-tagged ubiquitin (2.2 μg) and N-terminally FLAG-tagged Mdm2 (pSG-FLAG-Mdm2, 1.42 μg) or control empty vector (1.42 μg), were introduced into H1299 cells (6×10^5 cells/10-cm dish). Cells were harvested 27 h post-transfection. Cell lysates were prepared in the presence of 1 mg/ml *N*-methylmaleimide (Sigma) to avoid degradation of ubiquitinated p53. Ubiquitinated and nonubiquitinated p53 were immunoprecipitated with anti-p53 polyclonal antibody (FL393) and analyzed by Western blotting.

^{35}S Pulse-Chase—H1299 cells (4×10^5 cells/10-cm dish) were transfected with 4 μg of plasmids with a 1:9 ratio of pcDNA-p53-72P or 72R/pCMV-Myc-Mdm2. At 19.5 h after transfection, cells were starved for 30 min in methionine- and cysteine-free DMEM with dialyzed serum and then labeled with 4.1 MBq/ml EXPRE^{35}S^{35}S ^{35}S-protein labeling mix (PerkinElmer Life Sciences) for 30 min. Cells were then cultured for 1.5 h in chase medium containing 500 μg/ml methionine and 500 μg/ml cysteine. Following incubation, cells were collected at the indicated times. Whole cell lysates were prepared from the collected cells, and immunoprecipitation was performed using anti-p53 mouse monoclonal antibodies PAb1801 and PAb421, run on SDS-PAGE, and detected by autoradiography.

Analysis of p53 Single Nucleotide Polymorphism and the Copy Number of the mdm2 Gene by Array-based Comparative Genomic Hybridization—To analyze p53 single nucleotide polymorphisms, a 10- or 20-ml whole blood sample was obtained from each individual. Genomic DNA was isolated and subjected to genotyping for p53 single nucleotide polymorphism by pyrosequencing, as described previously (19). For

Downloaded from www.jbc.org at KOKURITSU GAN CENTER, on May 17, 2012

array-based comparative genomic hybridization, 62 surgical specimens of lung cancer patients who had been diagnosed and had undergone surgery at the National Cancer Center Hospital were analyzed by MCG cancer array-800 comparative genomic hybridization, as described previously (24). MCG Cancer array-800 is a custom-made array consisting of ~800 BACs harboring 800 known cancer-related genes, intended for diagnosis of cancer-specific copy number aberrations. When the signal ratio (test signal/reference signal) for the copy number of the *mdm2* gene was more than 1.25, it was defined as chromosomal gain. The threshold for chromosomal gain (ratio >1.25) was determined previously by "normal *versus* normal experiments" (24).

RESULTS

N-terminal Structures of p53-72P and -72R Protein Are Different—The polymorphism of p53 at codon 72 was first reported over 2 decades ago as a non-tumor-derived amino acid change that altered the mobility of p53 on SDS-polyacrylamide gels (14–16). As shown in supplemental Fig. S1, *A* and *B*, altered mobilities of ectopically expressed, endogenously expressed, and purified p53-72P and -72R were similarly detected by Western blotting. Because purified p53 proteins prepared from *E. coli* do not undergo post-translational modifications (data not shown), the altered mobility is not due to such modifications but to the intrinsic nature of the proteins. It has been suggested that this altered mobility reflects the altered structure of the protein by amino acid change; however, because structural information about this domain is lacking, this hypothesis has not been tested. We therefore tried to test this hypothesis by partial proteolytic digestion of purified p53-72P and -72R protein. When a protein is partially digested by proteases, a difference in the protein structure is detected as sensitivity to protease digestion at each cleavage site. To observe intrinsic differences between p53-72P and -72R proteins, we used purified proteins prepared from *E. coli*. As shown in Fig. 1*A*, the products of partial proteolysis by subtilisin were analyzed by Western blotting using anti-p53 antibodies, detecting different positions within the p53 protein. We first recognized that fragments showing altered mobility between p53-72P and -72R were detected even after proteolytic digestion (Fig. 1*A*, *open circles*). Such fragments were frequently detected by the antibody detecting N-terminal p53 (Pab1801), and this demonstrates that N-terminal fragments contain a region causing electrophoretic mobility differences. However, when the antibody detecting C-terminal p53 was used (Pab122), most fragments showed the same migration, showing that the C-terminal portion of p53-72P and -72R is indistinguishable by SDS-PAGE. In addition to these fragments, the analysis revealed two bands detected only in p53-72R (Fig. 1*A*, 22- and 34-kDa bands, shown with *arrows*). As shown in Fig. 1*B*, most of the estimated digestion sites for these bands lie within the N-terminal half of p53, demonstrating that a difference in protease accessibility is frequently observed in the N-terminal p53. We also performed the same experiment using Pab240 (which detects 211–220 amino acids of p53 protein), and we found that the 22-kDa band is not detected by Pab240, suggesting the N-terminal origin of the fragment (data not shown). Unfortunately, several bands appeared around 34 kDa, and we could not verify whether a

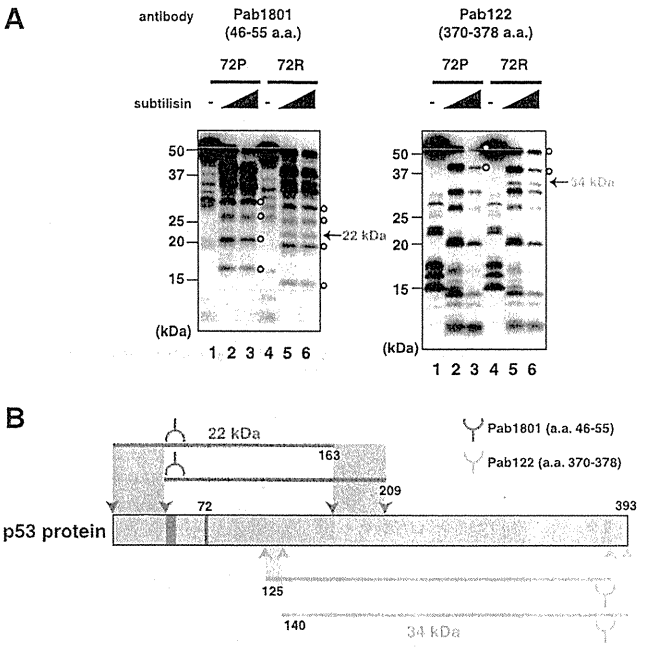

FIGURE 1. **Partial proteolytic digestion of purified p53-72P and -72R.** *A*, 35 ng of purified p53-72P or -72R were digested with subtilisin at 0.5 μg/ml (*lanes 2* and *5*) and at 1 μg/ml (*lanes 3* and *6*) for 30 min on ice. Products were resolved by 15–25% SDS-PAGE and analyzed by Western blotting using the indicated antibodies. Bands with a different proteolytic pattern (specifically observed for p53-72R) are shown by *arrows*. Note that when using antibody against N-terminal positions of p53 (Pab1801), fragments showing altered mobility on the gel between p53-72P and -72R are frequently detected (*open circles*). *B*, estimated digestion sites for p53-72R-specific bands. Schematic representation of p53 protein (*gray*) together with recognition sites for Pab1801 (*green*) and Pab122 (*yellow*) is shown. Polymorphic codon 72 is shown in *red*. The *upper two green bars* (22-kDa band in *panel Pab1801*) and *lower two yellow bars* (34-kDa band in *panel Pab122*) are the estimated alignments of p53-72R-specific fragments. The estimated amino acid numbers of the fragments were calculated according to the molecular weight of the fragments. The fragments were detected by antibodies and therefore should be derived from somewhere between the two bars. It can be assumed that p53-72R-specific digestion occurred between the *arrowheads*.

34-kDa p53-72R-specific band is detected by Pab240 (data not shown). These results collectively indicate that differences in protein structure are mainly detected in the N-terminal portion of p53.

Phosphorylation in N-terminal p53 Is Enhanced in p53-72R Compared with -72P—We next speculated that the difference in the protein structure between the variants might affect the association with the kinases that phosphorylate p53. Because the structural differences of p53-72P and -72R are mainly detected in the N-terminal region, we analyzed the phosphorylation levels of p53-72P and -72R within the N-terminal domain. We reasoned that subtle differences between the variants become evident only when they are expressed within cells having the same genetic background; therefore, we analyzed the phosphorylation levels of p53-72P and -72R by transfecting them into a cell line with no p53 (Saos2 cells). In addition, to exclude the possibility that p53 expressed in the cells is unnaturally high, each p53 was expressed from a weak retroviral LTR promoter. As shown in Fig. 2, phosphorylation levels of p53-72P and -72R were similar on Ser-9, -15, -37, and -46. However, significantly enhanced phosphorylation of 72R compared with 72P at Ser-6 and -20 was detected. Phosphorylation in the

Downloaded from www.jbc.org at KOKURITSU GAN CENTER, on May 17, 2012

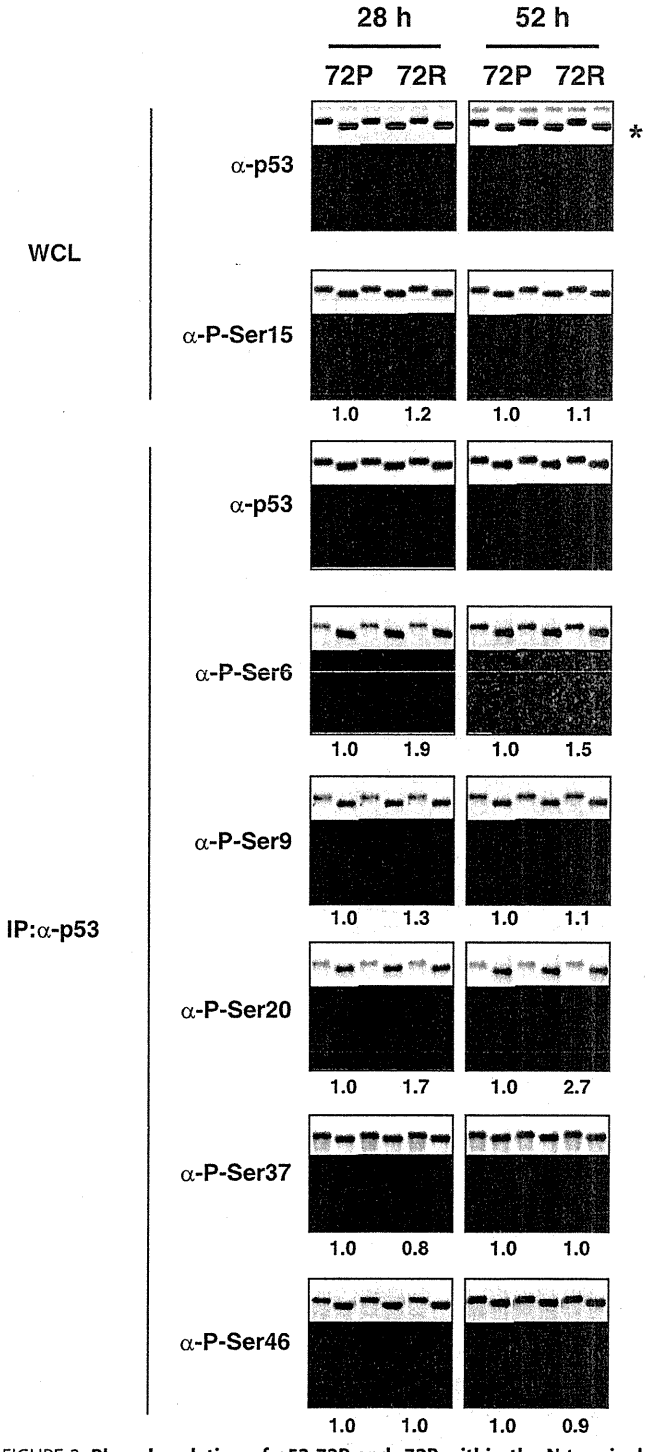

FIGURE 2. **Phosphorylation of p53-72P and -72R within the N-terminal transactivation domain.** Saos2 cells (4.4×10^6 cells/10-cm dish) were transfected with pMX-p53-72P or -72R (1.78 μg), and harvested 28 and 52 h post-transfection. To detect the phosphorylation of p53 efficiently (except Ser-15), p53 proteins were immunoprecipitated (*IP*) using anti-p53 antibodies (anti-p53 mouse monoclonal antibody pAb1801 and pAb421 were mixed). Total p53 and phosphorylated p53 were analyzed by Western blotting. The experiment was repeated three times, and representative images are shown. The phosphorylation levels of p53-72P and -72R were quantified using Image J software. Relative phosphorylation levels (normalized by total p53) are shown *below* the panels. *Asterisk* denotes a nonspecific band. *WCL*, whole cell lysate.

N-terminal region of p53 is closely related with p53 activity. We therefore analyzed whether enhanced phosphorylation at Ser-6 and -20 in p53-72R results in enhanced tumor-suppressing function of the protein, as shown below.

Stability of p53-72R Is Increased Compared with p53-72P—Phosphorylation at Ser-20 mediates the stabilization of the p53 protein by inhibiting p53-Mdm2 interaction (11). Because we detected enhanced phosphorylation at Ser-20 in p53-72R compared with p53-72P, we focused on the stability of p53 proteins expressed within the cell. We first expressed the variants at different expression levels (200–1200 ng of p53 expression vectors transfected per 10-cm dish). We speculated that if the differences in protein levels were due to differences in degradation levels by endogenous Mdm2, increased expression of p53 would override degradation by Mdm2. As shown in Fig. 3*A*, when both p53s were expressed at relatively high levels (800 or 1200 ng of p53 expression vectors transfected per 10-cm dish), no difference in total p53 levels was detected, whereas when the expression levels were decreased (200 or 400 ng transfected), p53-72R was expressed at a significantly higher level than p53-72P. The mRNA expression levels of both variants were similar even when p53-72R protein was expressed at a significantly higher level than p53-72P protein in H1299 and Saos2 cells (Fig. 3*B*); therefore, the difference in the p53 protein amount is regulated at the post-transcriptional level. We further tested whether this difference could be detected in cells lacking Mdm2. We utilized *p53* and *mdm2* double-deficient mouse embryonic fibroblasts (*p53*/*mdm2* DKO)[3] for this purpose. As shown in Fig. 3*C*, no difference in p53 protein levels was detected in *p53*/*mdm2* DKO (under the conditions utilized, expression levels of p53 variants were similar or lower than in H1299 cells, data not shown).

We next tested whether the difference in protein expression levels was affected by phosphorylation at Ser-20, which was converted to alanine in p53-72P and -72R to obtain nonphosphorylatable p53 at Ser-20 (therefore is degradable by Mdm2), and expressed in H1299 and *p53*/*mdm2* DKO. As shown in Fig. 3*D*, significant decreases in protein levels were detected for S20A mutants compared with wild-type p53s in H1299 cells. However, no such decreases were detected in *p53*/*mdm2* DKO, indicating that diminished expression levels of S20A mutants in H1299 is a result of enhanced degradation of the mutants by Mdm2. The level of S20A mutant for p53-72P was still slightly lower than p53-72R in H1299 cells, demonstrating that, in addition to phosphorylation at Ser-20, other factors may affect the difference in protein expression levels. Collectively, these results suggest that the difference in p53 protein expression levels is the result of a difference in the degradation levels of p53-72R and -72P by Mdm2, and this difference has been brought about at least partly from differences in phosphorylation levels at Ser-20.

Mdm2 Degrades p53-72P More Efficiently than p53-72R—We further tested whether there is a difference in protein degradation by Mdm2 between polymorphic variants. We first co-transfected Mdm2 with p53-72R or -72P in H1299 cells. As

[3] The abbreviations used are: DKO, double KO; ca., constitutively active.

Downloaded from www.jbc.org at KOKURITSU GAN CENTER, on May 17, 2012

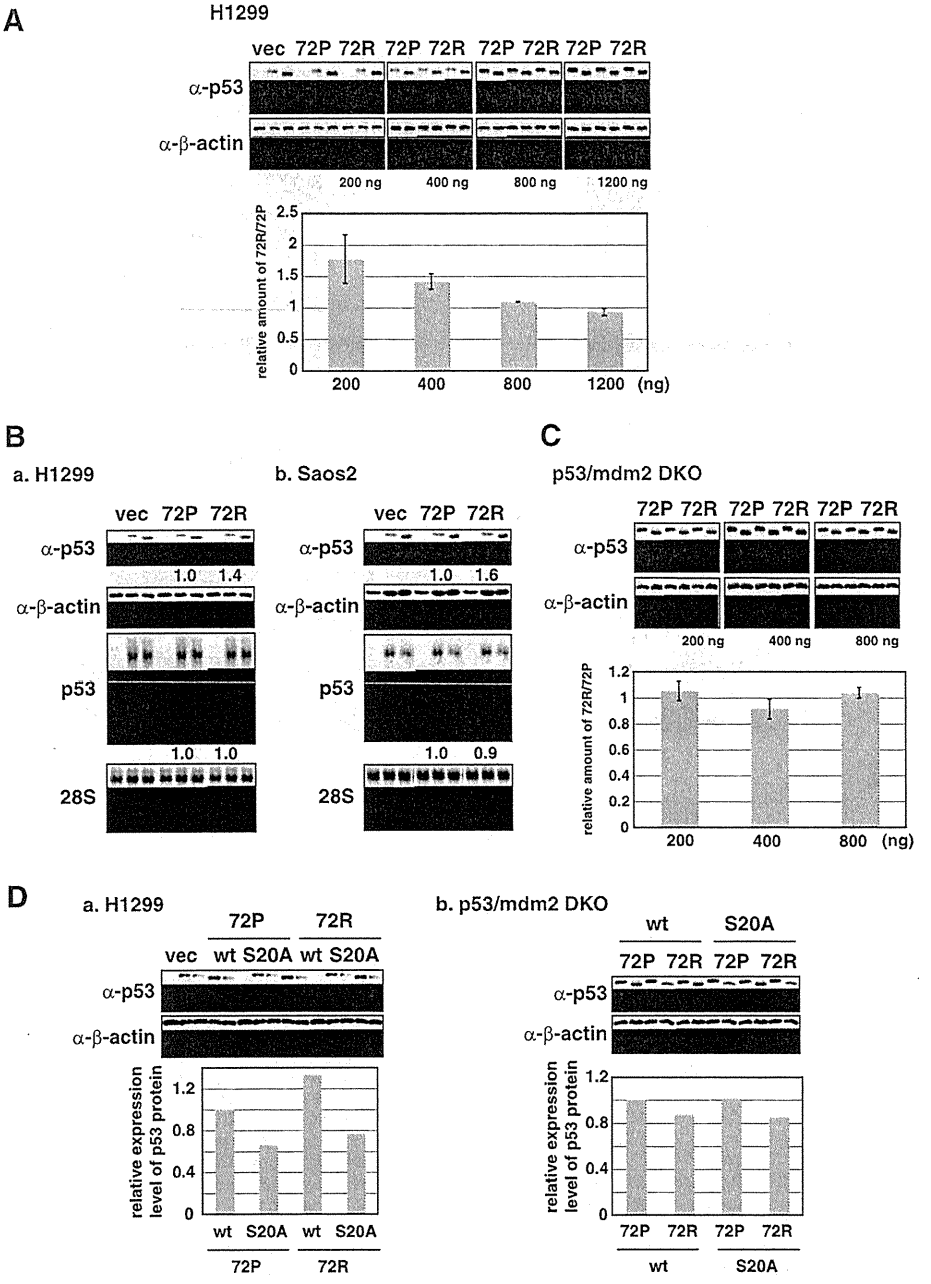

FIGURE 3. **Expression level of p53-72R protein is higher than p53-72P protein.** *A,* indicated amounts of pMX-p53-72P or -72R expression plasmids were introduced into H1299 cells (4.4×10^5 cells/10-cm dish). Cells were harvested 27 h post-transfection and analyzed by Western blotting. Experiments were performed in triplicate, and representative images are shown. The levels of p53 and β-actin were quantified using Image J software, and p53 levels were normalized by β-actin levels. The mean ± S.D. of relative p53-72R/p53-72P levels was calculated and is shown in the *bottom column. vec,* vector. *B,* p53 protein and mRNA levels were analyzed by Western and Northern blotting. The levels of p53 protein (normalized by β-actin levels) and mRNA (normalized by 28 S levels) were quantified using Image J software. *Panel a,* pMX-p53-72P or -72R (0.2 μg) was introduced into H1299 (4.4×10^5 cells/10-cm dish). Cells were harvested 27 h post-transfection. *Panel b,* pMX-p53-72P or -72R (0.9 μg) was introduced into Saos2 cells (4.4×10^6 cells/10-cm dish). Cells were harvested 24 h post-transfection. *C,* indicated amounts of pMX-p53-72P or -72R expression plasmids were introduced into *p53/mdm2* DKO (4.4×10^5 cells/10-cm dish) and analyzed as in *A. D,* expression plasmids (cloned in pMX vector) of wild-type or mutant (S20A) p53-72P or -72R were introduced into H1299 (in *panel a*, 4.4×10^5 cells/10-cm dish, 500 ng transfected) or *p53/mdm2* DKO (in *panel b*, 4.4×10^5 cells/10-cm dish, 200 ng transfected) cells. Cells were harvested 21 h (*panel a*) or 27 h (*panel b*) post-transfection. Experiments were performed in duplicate, and the mean values of relative p53-72P and -72R levels are presented.

shown in Fig. 4*A*, although p53-72P was efficiently degraded under the conditions tested, p53-72R was resistant to degradation. We further analyzed the ubiquitination of both variants by Mdm2. His-tagged ubiquitin was co-expressed with p53 and Mdm2 in H1299 cells. Cell lysates were prepared, and p53 was immunoprecipitated by anti-p53 antibody. Immunoprecipitates were analyzed by Western blotting using anti-His tag antibody. As shown in Fig. 4*B*, it was shown that His-tagged ubiquitinated p53 was more prominent in p53-72P than p53-72R. We also performed a nickel pulldown assay under denaturing conditions to purify His-tagged ubiquitinated proteins. The samples were then analyzed by Western blotting using anti-p53

Downloaded from www.jbc.org at KOKURITSU GAN CENTER, on May 17, 2012